Comparison of optical and microphysical properties of pure Saharan mineral dust observed with AERONET Sun photometer, Raman lidar, and in situ instruments during SAMUM 2006

D. Müller,[1,2] K.-H. Lee,[1] J. Gasteiger,[3] M. Tesche,[4] B. Weinzierl,[5,6] K. Kandler,[7] T. Müller,[2] C. Toledano,[8,9] S. Otto,[10,11] D. Althausen,[2] and A. Ansmann[2]

Received 2 September 2011; revised 13 January 2012; accepted 15 January 2012; published 14 April 2012.

[1] The Saharan Mineral Dust Experiment (SAMUM) 2006, Morocco, aimed at the characterization of optical, physical, and radiative properties of Saharan dust. AERONET Sun photometer, several lidars (Raman and high-spectral-resolution instruments), and airborne and ground-based in situ instruments provided us with a comprehensive set of data on particle-shape dependent and particle-shape independent dust properties. We compare 4 measurement days in detail, and we carry out a statistical analysis for some of the inferred data products for the complete measurement period. Particle size distributions and complex refractive indices inferred from the Sun photometer observations and measured in situ aboard a research aircraft show systematic differences. We find differences in the wavelength-dependence of single-scattering albedo, compared to light-scattering computations that use data from SOAP (spectral optical absorption photometer). AERONET data products of particle size distribution, complex refractive index, and axis ratios were used to compute particle extinction-to-backscatter (lidar) ratios and linear particle depolarization ratios. We find differences for these parameters to lidar measurements of lidar ratio and particle depolarization ratio. Differences particularly exist at 355 nm, which may be the result of differences of the wavelength-dependent complex refractive index that is inferred by the methods employed in this field campaign. We discuss various error sources that may lead to the observed differences.

Citation: Müller, D., et al. (2012), Comparison of optical and microphysical properties of pure Saharan mineral dust observed with AERONET Sun photometer, Raman lidar, and in situ instruments during SAMUM 2006, *J. Geophys. Res.*, *117*, D07211, doi:10.1029/2011JD016825.

1. Introduction

[2] This contribution is part three of our study [*Müller et al.*, 2010a, 2010b] of optical and microphysical properties of mineral dust observed during the Saharan Mineral Dust Experiment (SAMUM) 2006. The field experiment was carried out in Morocco.

[3] The main results of SAMUM 2006 are presented in a collection of papers in a special issue in Tellus, 61B, 2009. We operated three Raman aerosol lidars and two Sun photometers at Ouarzazate airport (30.93° N, 6.9° W, 1133 m above sea level (asl)) from 11 May until 10 June 2006 [*Tesche et al.*, 2009; *Toledano et al.*, 2009]. One of the Sun photometers was an Aerosol Robotic Network (AERONET) system [*Holben et al.*, 1998]. The second instrument was operated by the University of Munich.

[4] Optical and microphysical properties of Saharan mineral dust were inferred from observations of direct and diffuse solar radiation and the use of AERONET's latest mineral dust model [*Dubovik et al.*, 2006]. This model has been specifically designed for the analysis of particles of non-spherical shape. Spheroidal particle shape is assumed in the retrieval procedure.

[5] Airborne measurements were carried out with the Falcon aircraft between 18 May and 7 June 2006 [*Petzold et al.*, 2009; *Weinzierl et al.*, 2009]. The aircraft carried a high-spectral-resolution lidar [*Esselborn et al.*, 2009] which allowed us to sound the atmosphere in close vicinity around

[1]Atmospheric Remote Sensing Laboratory, School of Environmental Science and Engineering, Gwangju Institute of Science and Technology, Gwangju, South Korea.
[2]Leibniz Institute for Tropospheric Research, Leipzig, Germany.
[3]Meteorological Institute, Ludwig Maximilian University, Munich, Germany.
[4]Department of Applied Environmental Science, Stockholm University, Stockholm, Sweden.
[5]Institut für Physik der Atmosphäre, Deutsches Zentrum für Luft- und Raumfahrt, Wessling, Germany.
[6]Also at Fakultät für Physik, Ludwig Maximilian University, Munich, Germany.
[7]Institut für Angewandte Umweltwissenschaften, Technische Universität Darmstadt, Darmstadt, Germany.
[8]Grupo de Óptica Atmosférica, Universidad de Valladolid, Valladolid, Spain.
[9]Formerly at Meteorological Institute, Ludwig Maximilian University, Munich, Germany.
[10]Leipzig Institute for Meteorology, University of Leipzig, Leipzig, Germany.
[11]Formerly at Institut für Methodik der Fernerkundung, Deutsches Zentrum für Luft- und Raumfahrt, Wessling, Germany.

0148-0227/12/2011JD016825

Table 1. Data Products Compared in Our Study[a]

Investigated Parameters	Instrument				
	Raman Lidar Ground	HSRL Aircraft	AERONET Ground	In Situ Aircraft	In Situ Ground
Extinction coefficient	x	x	x	x	-
Scattering coefficient	-	-	x	x	-
Absorption coefficient	-	-	x	x	-
Ångström exponent	x	-	x	x	-
Extinction-to-backscatter (lidar) ratio	x	-	x	-	-
Linear particle depolarization ratio	x	x	x	-	-
Single-scattering albedo	-	-	x	-	x
Particle size distribution	-	-	x	x	x
Complex refractive index (real part)	-	-	x	x	x
Complex refractive index (imaginary part)	-	-	x	x	x
Particle aspect ratio	-	-	x	x	x

[a]All parameters except for the particle size distribution and the aspect ratio are presented as wavelength-dependent quantities. The wavelengths for which we carried out the analysis are given in the figure captions of this contribution. Instruments and data analysis are described by *Tesche et al.* [2009], *Esselborn et al.* [2009], *Freudenthaler et al.* [2009], *Heese et al.* [2009], *Müller et al.* [2009, 2010a, 2010b], *Weinzierl et al.* [2009], and *Kandler et al.* [2009]. Regarding the Raman lidar measurements, we calculated the Ångström exponents from the profiles of the extinction coefficients measured with Raman lidar. Regarding the AERONET Sun photometer and the in situ aircraft measurements, we computed the Ångström exponents from particle extinction, scattering, and absorption coefficients. Details are given in section 3.

the ground station. Aircraft measurements provide us with particle size distributions in the size range up to 30 μm radius. Chemical analysis of thousands of particles collected aboard the aircraft allowed us to compute the complex refractive index and the axis ratio distribution of the particles [*Kandler et al.*, 2009]. We measured with lidar the particle extinction coefficients at 355 and 532 nm, and thus the extinction-related Ångström exponent for this wavelength pair. Both parameters are less influenced by particle shape. We also measured particle backscatter coefficients, lidar ratios, and linear particle depolarization ratios, which significantly depend on particle shape.

[6] To date we lack in high-quality experimental field data that allow us to test the robustness of light-scattering models of mineral dust. *Müller et al.* [2010a] present a comparison of optical parameters of mineral dust for which particle shape may not be so important in the measurement process, respectively, the retrieval procedure. *Müller et al.* [2010a] and *Müller et al.* [2010b] present results of one measurement case only. We selected 19 May 2006. It was the day for which we had data from all measurement platforms.

[7] We compared data products acquired with Raman and high-spectral resolution lidar, Sun photometer and airborne and ground-based in situ instrumentation. One purpose of our study was to test the quality of the derived data products. Measurement and data analysis techniques employed in this campaign are affected by particle shape. Thus, differences of the same data product inferred by different measurement platforms may help in identifying if particle shape or other reasons may be responsible for the observed deviations.

[8] One striking result was that particle size distribution inferred from AERONET Sun photometer measurements and measured in situ aboard a research aircraft differed significantly [*Müller et al.*, 2010a]. We found that so-called shape-independent parameters, i.e. dust properties whose determination with the various instruments platforms depends little on the exact knowledge of particle shape agree reasonably well [*Müller et al.*, 2010a]. These parameters are particle extinction, scattering and absorption coefficients, the Ångström exponents that are associated with the three latter parameters, and single-scattering albedo. Particle shape-dependent parameters in contrast showed in part large differences, which may be caused by an insufficient knowledge of particle shape and/or the light-scattering models that were used in data analysis [*Müller et al.*, 2010b]. These parameters are particle extinction-to-backscatter (lidar) ratio, linear particle depolarization ratios, and aspect ratios of dust; in this latter case we approximate the complex shape of dust particles by spheroids.

[9] Drawback of our previous study is the fact that we used only one measurement day for the comparison study. At the time of our data analysis we did not have the set of parameters available for further studies. In the past 1.5 years we analyzed the data of the SAMUM 2006 campaign in a rather comprehensive fashion. We collected as many data as possible of the different measurement platforms and we carried out the comparison study for many more measurement days. A goal of our study is to find out if the results of *Müller et al.* [2010a, 2010b] can be generalized.

[10] In this contribution we present results of three more measurement cases in detail. We follow the procedures outlined by *Müller et al.* [2010a, 2010b]. We also provide a statistical analysis of the SAMUM 2006 results. We analyzed all measurement days of the different instrument platforms that can be used for our study. Table 1 summarizes the parameters that we compare.

[11] We also carried out light-scattering computations as an extension of the studies presented by *Wiegner et al.* [2009]. A goal of this work is to see if any combination of measured dust parameters allows us to reproduce some dust optical parameters, i.e., linear dust depolarization ratio and lidar ratio, which can be measured directly with lidar and without critical assumption on particle shape.

[12] Our study also expands on the publications by *Reid et al.* [2003, 2008]. The authors critically discuss results of measurements of mineral dust observed with AERONET Sun photometer and various in situ instrumentations. Observations were carried out in the Arabian Peninsula [*Reid et al.*, 2008], which is in the source regions of mineral dust emissions, and in Puerto Rico [*Reid et al.*, 2003], which is in the far-field of Saharan dust. The authors find considerable variation of dust size distributions. The authors critically discuss reasons for the observed variations. Some of the variations are likely due to the measurement

technique that is employed for the measurement of the particle size distributions. In other words, different measurement techniques may result in different results for the same particle size distributions.

[13] Another goal of our comparison study is to develop a particle light-scattering model for mineral dust. We want to apply it to the inversion of dust optical properties (measured with lidar) into dust microphysical properties, e.g., particle effective radius, volume, surface-area, and number concentration, and the complex refractive index. Until now we can infer these parameters from multiwavelength Raman lidar observations only if the particles are of spherical shape [*Müller et al.*, 1999a; *Veselovskii et al.*, 2002; *Böckmann et al.*, 2005].

[14] The light-scattering model that is used in the AERONET inversion algorithm is one potential candidate for our inversion method. However, this dust model has not been designed for describing light-scattering properties at 180°. Some of the data products presented here are not a standard output of the AERONET retrieval scheme, but they can be comparably easily calculated from particle size distribution, complex refractive index, and aspect ratio [*Dubovik et al.*, 2006]. Just recently this light-scattering model has, for the first time, been tested in the inversion of multiwavelength lidar data [*Veselovskii et al.*, 2010].

[15] We are currently carrying out studies with the inversion methodology of *Veselovskii et al.* [2002]. We use the concept of the AERONET light-scattering model. Our test data set consists of several measurement cases of SAMUM 2006 and data taken during the follow up campaign SAMUM 2008 [*Ansmann et al.*, 2011]. The interpretation of the inversion results will also rest upon the findings of our study made here and the previous two contributions by *Müller et al.* [2010a, 2010b].

[16] In section 2 we summarize the instruments and the methods. In section 3 we present results of several measurement days in more detail. In section 4 we present a statistical overview on the results of SAMUM 2006. We summarize our results in section 5. We close in section 6 with an outlook on new methodologies that could further improve our understanding of mineral dust properties.

2. Methodology

[17] We briefly summarize the measurement techniques. Instruments, data analysis methods, and error estimates are described in detail in the individual papers of the first special issue on SAMUM (Tellus, 61B, 2009), and by *Müller et al.* [2010a, 2010b].

[18] We carried out collocated observations with an AERONET Sun photometer [*Holben et al.*, 1998, 2001] and three Raman lidars at Ouarzazate airport. One lidar instrument was the Backscatter Extinction lidar-Ratio Temperature Humidity profiling Apparatus (BERTHA) of the Leibniz Institute for Tropospheric Research (IfT) [*Althausen et al.*, 2000; *Tesche et al.*, 2009]. Two more systems, the three-wavelength Multiwavelength Lidar System (MULIS) [*Freudenthaler et al.*, 2009] and the one-wavelength Portable Lidar System (POLIS) [*Freudenthaler et al.*, 2009] were operated by the University of Munich. A fourth lidar system was operated aboard the DLR (German Aerospace Center) research aircraft Falcon. This lidar is a high-spectral-resolution lidar (HSRL) [*Esselborn et al.*, 2009]. The aircraft passed over the Ouarzazate ground station on several days during SAMUM. *Müller et al.* [2010a, Table 2] summarize the data products that were measured with the lidar systems. Details of data analysis and error analysis are described by *Tesche et al.* [2009], *Freudenthaler et al.* [2009], *Esselborn et al.* [2009], and *Heese et al.* [2009].

[19] The AERONET instrument measured the direct radiation of the Sun at 339, 379, 441, 501, 675, 869, 940, 1021, and 1638 nm wavelength. Sky radiance (almucantar) measurements were carried out at 441, 501, 675, 869, 1021, and 1638 nm. The instrument was calibrated at NASA Goddard Space Flight Center (GSFC) before and after the field campaign. The accuracy of the aerosol optical depth measurements is approximately 0.01 at visible and near infrared wavelengths and approximately 0.02 in the ultraviolet wavelength region [*Eck et al.*, 1999].

[20] Aerosol optical depth, aerosol phase function, particle volume size distribution from 0.05–15 μm in radius, and the complex refractive index in the range from 1.33–1.6 (real part) and from $0.0005i$–$0.5i$ (imaginary part) were derived from the data. The algorithm is described by *Dubovik and King* [2000] and *Dubovik et al.* [2006]. From the retrieved data products we calculated all other parameters we use in our study, i.e., particle backscatter coefficients, lidar ratios, and linear particle depolarization ratios [*Müller et al.*, 2010b]. The instrument was equipped with a novel measurement channel at 1638 nm. We expect this channel to improve the retrieval accuracy of some of the data products, as for instance the particle size distribution.

[21] Another important output parameter of our study is the aspect ratio. Particles of spheroidal shape are assumed in the analysis of the AERONET data. The aspect ratio is defined as the ratio of the longest axis of a spheroid to its shortest axis; note that these two axes need to be chosen such that both axes are perpendicular to each other. Thus, the aspect ratio is always ≥ 1. In contrast, the axis ratio is defined by *Dubovik et al.* [2006] as the ratio between the length of the rotational axis to the length of the axis perpendicular to it. The axis ratio is <1 for flat spheroids, and >1 for elongated spheroids.

[22] We point out to some additional error sources. The data were analyzed by the AERONET team and provided to us directly. The results may therefore differ from the level 2 results in the AERONET database. Reason for this approach was that we had the opportunity to incorporate the novel measurement channel at 1638 nm. The data taken with the 1638-nm channel were added in the signal processing chain. The data at 339 and 379 nm were not provided to us.

[23] The accuracy of the calibration of this channel at 1638 nm is generally worse than for the other channels in the visible spectrum. A comparison of data products inferred with and without the new channel shows that additional errors are comparably low in view of all other error sources. We refer also to our previous publications in which we present retrieval results with and without this novel measurement channel [*Müller et al.*, 2010a, 2010b]. We emphasize that this channel still is not part of the standard data analysis chain of level 2 data, and therefore the results presented here may differ from a future level 2 data analysis.

[24] Another source of error in our data analysis may be low optical depth which prevailed on several of the measurement days such as 19 May and 4 June 2006. In order to

qualify for level 2 data analysis, optical depth must be greater than 0.4 at 440 nm and the solar zenith angle must be larger than 50° during the measurement. It is clear that this constraint of high optical depth was not met in many cases during the measurement period [see, e.g., *Müller et al.*, 2010a, Figure 1]. In nearly all of the analyzed cases optical depth was larger than 0.2 at 440 nm. Thus it was also necessary to have the analysis done by the AERONET team directly, as it may reduce some of the problems in the quality of the retrieval results.

[25] The research aircraft Falcon carried the nadir-looking HSRL and instruments for observations of aerosol particle microphysical and chemical properties. The instruments are described by *Petzold et al.* [2009], *Weinzierl et al.* [2009], and *Kandler et al.* [2009]. We operated another ground-based station at Tinfou (30.2° N, 5.6° W) for collection and chemical analysis of the particles from which we inferred the complex refractive index [*Kandler et al.*, 2009] and single-scattering albedo [*Müller et al.*, 2009].

[26] We used scanning electron microscopy to determine the aspect ratios of the collected particles as a function of particle size and flight level of the aircraft [*Kandler et al.*, 2009]. The aspect ratio was determined from an ellipse that was fitted into the two-dimensional particle outline measured by the electron microscope. We rotated the ellipse around its longest half-axis, thus, the axis ratio is always ≥1.

3. Case Studies: 19 and 28 May 2006, and 3 and 4 June 2006

[27] Table 2 lists the measurement times of the different instruments on 19 and 28 May and 3/4 June 2006. *Knippertz et al.* [2009] present an overview on the meteorological situation. Details on the measurement situation, data acquisition and analysis are found in the publications by *Tesche et al.* [2009] (BERTHA), *Esselborn et al.* [2009] (HSRL), *Freudenthaler et al.* [2009] (MULIS), *Heese et al.* [2009] (POLIS), *Müller et al.* [2010a, 2010b] (AERONET), *Weinzierl et al.* [2009] (airborne particle size distribution measurements), *Kandler et al.* [2009] (chemical analysis of particles collected aboard the Falcon aircraft and at ground at Tinfou), and *Müller et al.* [2009] (ground-based measurements of particle absorption with SOAP).

[28] The three ground-based Raman lidar systems have different overlap functions [*Wandinger and Ansmann*, 2002], and we obtain different minimum heights above which trustworthy particle extinction profiles can be derived. We can largely compensate for this overlap effect by combining the profiles of the three lidar systems. The airborne HSRL allows us to cross-check the quality of the profiles acquired by the ground-based lidar measurements at 532 and 1064 nm, as the profiles reach down to the ground.

[29] Figure 1 illustrates the measurement situation. Time-altitude plots of the range-corrected signals show the variability of the dust layer height on these four days. We selected the wavelength at 710 nm as it is comparably sensitive to the presence of dust particles. We also determined extinction profiles from measurements of Raman signals taken during the measurement times shown in Figure 1. The extinction coefficient profiles are shown on the left part of each time-altitude plot. We also show mean values of the particle extinction coefficient measured with MULIS and the airborne HSRL, and the column-mean extinction coefficient that we derived from the AERONET Sun photometer measurements. The measurements were carried out either before or after the aircraft overflights. The scaling height of Sun photometer optical depth was determined with lidar signals taken closest in time to the Sun photometer observations.

[30] The profiles serve as an indicator whether it is reasonable to compare data products from Sun photometer (column-averaged and column-integrated data products), lidar (vertical profiles), and airborne in situ measurements (carried out in various height levels). It is quite clear that a match of intensive and extensive parameters is less likely to occur for the different measurement platforms, if observation geometry and/or observation time differ, see also the discussion by *Müller et al.* [2010a, 2010b]. Regardless of the proximity of BERTHA and MULIS, and the fact that the airborne HSRL passed over the Ouarzazate field site it is obvious that all three instruments sounded different portions of the dust plume on the four measurement days. An extinction coefficient that changes with height is a strong indicator of vertically varying extensive properties.

[31] Extinction coefficients were measured with BERTHA, MULIS, and HSRL at 532 nm. We find a good agreement for the extinction coefficients to heights as low as 1.5 km asl on 19 May 2006. Differences are at maximum 20% in the height interval around 4 km height and otherwise considerably less. Regarding the measurement on 28 May 2006 we find good agreement for the profiles above 3 km height asl. We find deviations of less than 15% in the plume between 2.8 and 3.6 km height. Below 2.4 km height we could not measure extinction coefficients with BERTHA. On 3 June, the extinction values measured with the three instruments scatter by as much as 50% in each height level. Nevertheless, we still see similar structures in the extinction profiles, i.e., a dust layer with increased extinction values reaches up to approximately 3 km height asl. On top of this layer we find another layer with lower extinction coefficients up to 4.5 km asl. Regarding the measurement on 4 June 2006 we find comparably good agreement between the profiles measured with MULIS and HSRL. The extinction coefficients measured with BERTHA below 3 km asl are systematically lower.

[32] Note that only BERTHA and HSRL measured extinction profiles on 3 June. The profiles from MULIS are obtained by the Klett solution of the backscatter coefficient [*Tesche et al.*, 2009]. The height-dependent lidar ratio used in the transformation from profiles of the backscatter to profiles of the extinction coefficients seems to be chosen improperly in the upper part of the dust layer. The HSRL profile furthermore represents an average over 5 s only, compared to 40, 100, and 13 s averaging intervals on 19 May, 28 May, and 4 June, respectively.

[33] We also show the time series of optical depth measured with the AERONET Sun photometer and the extinction-related Ångström exponents that can be inferred from the optical depth data. Regarding the extinction-related Ångström exponent we need to consider that lidar measures particle extinction at 355 and 532 nm, whereas the AERONET measurement wavelengths nearest to the lidar wavelengths are 441 and 501 nm. Thus, any comparison will suffer from this discrepancy in measurement wavelengths. A second order fit of the logarithm of aerosol optical depth versus the logarithm of the measurement wavelength is the

Table 2. Measurement Days and Measurement Times (in UTC) of the Different Instrument Platforms That are Used for Comparison Study in Section 3[a]

	Parameter: From Lidar and Sun Photometer According to Table 1			Parameters: ext, scat, abs, å, psd, cri_{NP}, Instrument: In Situ (Airborne), Measurement Time: Flight Level[b]	Parameter: cri_{CA}, Instrument: In Situ (Airborne), Measurement Time: Flight Level
Day	Instrument: Raman Lidar (ground), Lidar: Measurement Time	Instrument: HSRL (Airborne), Measurement Time	Instrument: AERONET (Ground), Measurement Time		
19 May	[1] BERTHA: 09:59–11:16 [2] MULIS: 11:04–11:14 [3] POLIS: 10:59–11:19 comparison time: around 11:00	10:50–11:13 overpass time: [4] 11:08 (40 s)[c]	[5] 06:49:19 [6] 07:11:50 [7] 08:01:35 [8] 08:29:46	[9] 11:23:44–11:37:44: 4853 m (L02) [10] 11:44:02–12:06:28: 3247 m (L03)	[11] 11:24:36–1:28:30: 4555 m [12] 11:24:36–11:45:00: 4555 m (with descent to 3040 m)
28 May	[13] BERTHA: 09:53–13:15 [14] MULIS: 10:37–10:49 [15] POLIS: in Tinfou comparison time: 10:41–10:43	10:35–11:15 overpass time: [16] 10:46 (100 s)	[17] 06:44:51 [18] 07:09:00 [19] 07:58:59 [20] 08:27:16	[21] 12:42:42–12:49:47: 3870 m (L10) [22] 12:52:02–12:54:02: 2907 m (L11) [23] 12:55:57–12:59:07: 2194 m (L12)	[24] 11:27:50–11:30:50: 3035 m [25] 11:41:53–11:46:00: 1815 m [26] 11:52:00–11:56:10: 1212 m
3 June	[27] BERTHA: 03:56–04:26 [28] MULIS: 04:12–04:16 [29] POLIS: 04:12–04:16 comparison time: 04:00–05:00	03:12–03:20 07:25–07:42 overpass time: [30] 03:15 (5 s) [31] 04:14 (5 s)	[32] 06:43:32 [33] 07:07:49 [34] 07:57:58 [35] 08:26:28	[36] 03:39:53–03:44:53: 3798 (L04) [37] 03:46:41–03:56:45: 2855 (L05) [38] 09:01:43–09:03:04: 2487 (L07) [39] 09:04:16–09:05:04: 2356 (L08)	[40] 08:20:07–08:24:30: 3648 m [41] 08:31:30–08:34:30: 2428 m [42] 08:45:30–08:49:00: 1127 m (ascent to 1172 m)
4 June	[43] BERTHA: 09:24–12:25 [44] MULIS: 08:53–13:15 [45] POLIS: 09:24–11:25 comparison time: 09:24–10:29 and 10:40–11:34[d]	09:35–09:51 10:46–11:25 overpass time: 09:48 and [46] 10:47 (10 s)	[47] 06:43:24 [48] 07:07:41 [49] 07:57:59	[50] 10:08:18–10:10:02: 3854 (L03) [51] 10:12:26–10:20:02: 2895 (L04) [52] 10:24:14–10:31:22: 1928 (L05)	[53] 11:45:50–11:48:20: 1821 m [54] 11:41:45–11:45:50: 3439 m (descent to 1832)

[a]Each data set is denoted by a number in brackets. These numbers are used to identify symbols shown in the figures of this section. Overpass time denotes the time at which the Falcon aircraft passed over the field site in Ouarzazate. Parameter abbreviations: ext, extinction coefficient; scat, scattering coefficient; abs, absorption coefficient; å, Ångström exponent derived from extinction, scattering, and absorption coefficients that were computed from particle size distributions and complex refractive indices; psd, particle size distribution; cri_{NP}, complex refractive index derived from measurements with nephelometer and PSAP according to *Petzold et al.* [2009]; and cri_{CA}, complex refractive index derived from chemical analysis of individual particles according to *Kandler et al.* [2009]. We also determined cri_{CA} from ground-based measurements at Tinfou; see Figure 3 and explanation in the text.

[b]The flight level is given in meter above ground. The numbers in brackets refer to Table 4 of *Weinzierl et al.* [2009].

[c]Numbers in brackets of overpass times denote duration of overpass, i.e., data collection time in seconds (s).

[d]Measurement times are given for BERTHA. Measurement times were 09:51–10:10 UTC and 10:55–12:15 UTC for MULIS and 09:24–10:16 UTC and 10:30–11:25 UTC for POLIS.

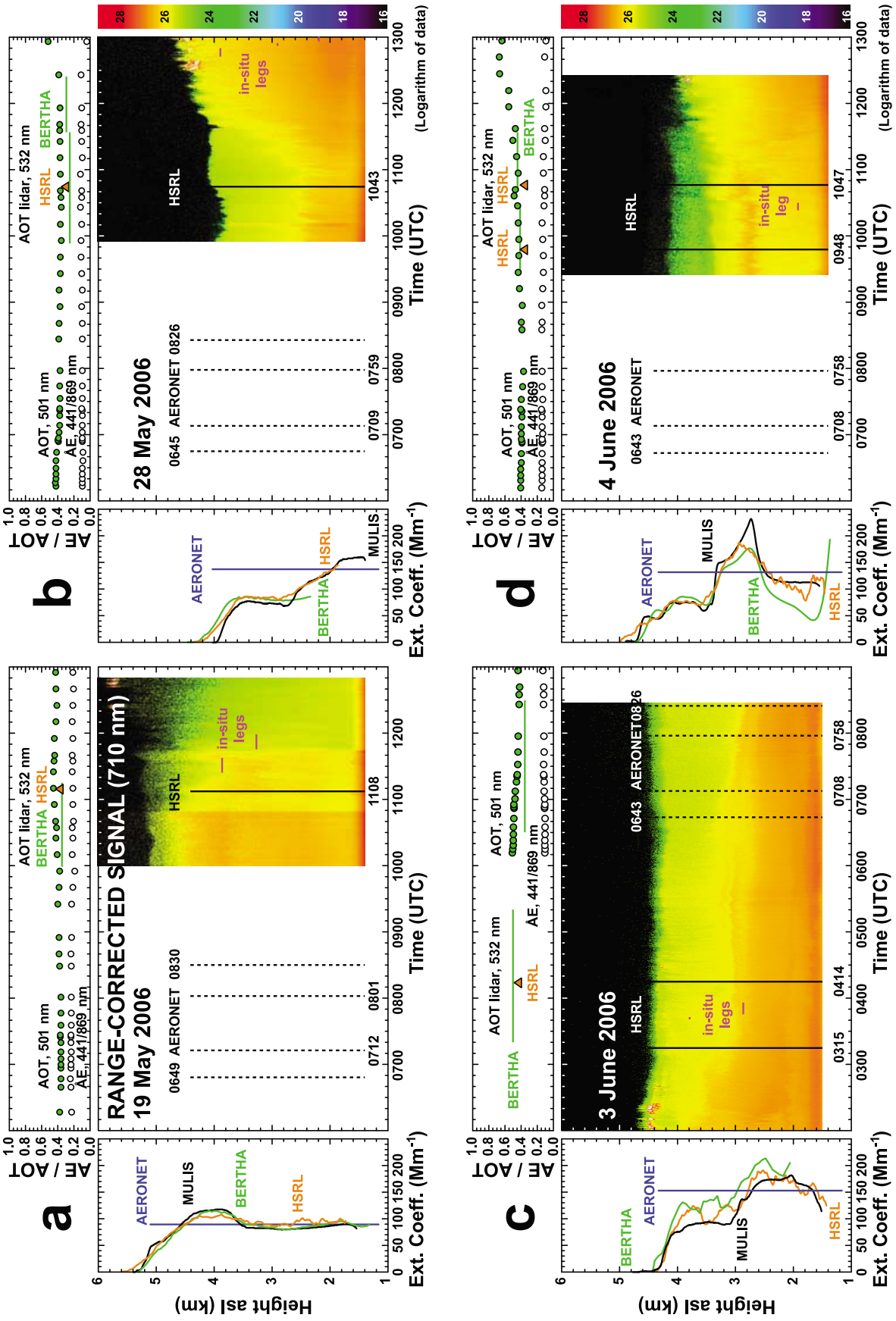
a
b
c
d
RANGE-CORRECTED SIGNAL (710 nm)
19 May 2006
28 May 2006
3 June 2006
4 June 2006
AOT lidar, 532 nm
AOT, 501 nm
AE, 441/869 nm
AERONET
MULIS
BERTHA
HSRL
in-situ legs
Height asl (km)
Ext. Coeff. (Mm-1)
Time (UTC)
AE / AOT
(Logarithm of data)

Figure 1

most accurate way to interpolate aerosol optical depth data to different wavelengths. With respect to the lidar data we think that such a sophisticated interpolation to the nearest measurement wavelengths of Sun photometer at 441 and 501 nm will not significantly improve our results. We have only data at two measurement wavelengths, and the measurement uncertainty of the lidar extinction coefficients is considerably larger than the accuracy of the optical depth measurements with Sun photometer.

[34] For the comparison we furthermore prefer to extrapolate the optical depth data taken with Sun photometer at 441 and 501 nm to the lidar measurement wavelengths. We selected this procedure for consistency reasons. For some of the lidar data products, i.e., particle lidar ratio and linear depolarization ratio the lidar instruments did not always provide us with results at 355 and 532 simultaneously. Therefore, using extrapolation of the Sun photometer data at least allows us to do a comparison even if the lidar data products are available at one measurement wavelength only.

[35] Figure 1 shows that optical depth and Ångström exponent did not change significantly during the measurement periods covered by Sun photometer and the lidar instruments (19 May, 28 May, and 4 June 2006). On 3 June 2006, optical depth slightly decreased between the nighttime lidar observations and the Sun photometer observations.

[36] The mean value of the 440/870-nm Ångström exponent was 0.12 on 4 June 2006. The standard deviation of ± 0.04 follows from 46 measurements taken between 0610 and 1542 UTC. The variation of the Ångström exponent was less on the other three days we use for our comparison. We find values of 0.22 ± 0.02 on 19 May, 0.1 ± 0.01 on 28 May, and 0.11 ± 0.04 on 3 June 2006. We assume that the Ångström exponent did not change significantly between nighttime and daytime observations on all four measurement days. We also see from Figure 1 that the Ångström exponent remained comparably stable during daytime.

[37] We find that optical depth from HSRL is lower by approximately 20% (19 May), 19% (28 May), and 18% and 24% (9:48 UTC and 10:47 UTC on 4 June) compared to optical depth from Sun photometer. Optical depth measured with BERTHA is lower than optical depth measured with the Sun photometer, too. Aerosol optical depth from the lidar measurements is determined by integration of the profile of the extinction coefficient. The lower values certainly cannot be explained by the difference in measurement wavelengths (501 nm for Sun photometer versus 532 nm for lidar), given the small wavelength dependence of particle extinction (see Figure 5). The parameter can show a low bias toward columnar AERONET measurements, when aerosol layers are missed in the integration process. This is the case, e.g., when extinction profiles do not extend all the way down to the surface as is the case for the profiles from the ground-based lidars shown in Figure 1. Extinction profiles from BERTHA are affected by the overlap effect while the ones from airborne HSRL measurements are very sensitive to the ground signal. The lowest point of the extinction profile is determined by the highest topographical feature within the averaging interval. Another source of bias is elevated layers which are not captured in the lidar measurements but included in columnar AERONET observation. The latter effect is negligible for SAMUM observations because the aerosol was restricted to the dust layer. Subvisible cirrus may pose a problem to an accurate retrieval of dust optical depth [*Huang et al.*, 2011]. Our analysis of the ground-based and airborne lidar data does not indicate that subvisible cirrus is responsible for the observed differences. Furthermore, our ground-based and airborne lidar observations do not indicate that aerosol layers above the dust layers contributed to total optical depth in a way that could explain the systematically larger aerosol optical depths from Sun photometer compared to optical depth from lidar.

[38] In summary, the information from our lidars and the Sun photometer leads us to the conclusion that the dust plumes were comparably stable (temporally) regarding particle intensive properties like effective radius, complex refractive index, and single-scattering albedo. This stability of the dust plumes is important for our purpose of testing the quality of some dust data products.

[39] The particle extinction coefficients varied with height (except on 19 May 2006). We need to consider this vertical variation in our comparison of extensive optical and microphysical particle properties measured by aircraft (in specific flight levels), by lidar (vertically resolved, respectively column-integrated), and by Sun photometer (column-mean and column-integrated data products).

3.1. Microphysical Parameters

[40] Figure 2 shows particle size distributions for the four measurement days. The results for 28 May and 3 and 4 June 2006 corroborate the findings for 19 May 2006 [*Müller et al.*, 2010a], i.e., particle size distributions from AERONET Sun photometer retrievals are different to the results from the Falcon in situ measurements.

[41] Inhomogeneities caused by variations of particle number concentration may be responsible for some of the observed differences. For this reason we scale our data for some of the following comparisons. In this way we avoid

Figure 1. Measurements with ground-based lidar (BERTHA) and Sun photometer, and airborne HSRL on (a, b) 19 and 28 May 2006, and (c, d) 3 and 4 June 2006. We show for each of the four measurement days: (1) Time series of particle optical depth at 501 nm (green dots) and particle extinction-related Ångström exponent (black circles) for the wavelength pair 441/869 nm from Sun photometer, optical depth from BERTHA (green line), and optical depth from HSRL (orange triangle); (2) profiles of the particle extinction coefficient at 532 nm from BERTHA, MULIS, HSRL, and mean extinction coefficients from the AERONET Sun photometer; and (3) the range-corrected backscatter signal at 710 nm measured with BERTHA. The measurement times of the AERONET Sun photometer are indicated by the vertical dashed lines. The overflight times of the HSRL are shown by the vertical solid line. The heights in which the in situ data were taken are shown by the horizontal magenta lines. The start and end of the horizontal lines shows the start and stop of the airborne measurements. AOT denotes aerosol optical depth and AE denotes the Ångström exponent (computed from optical depths respective extinction coefficients).

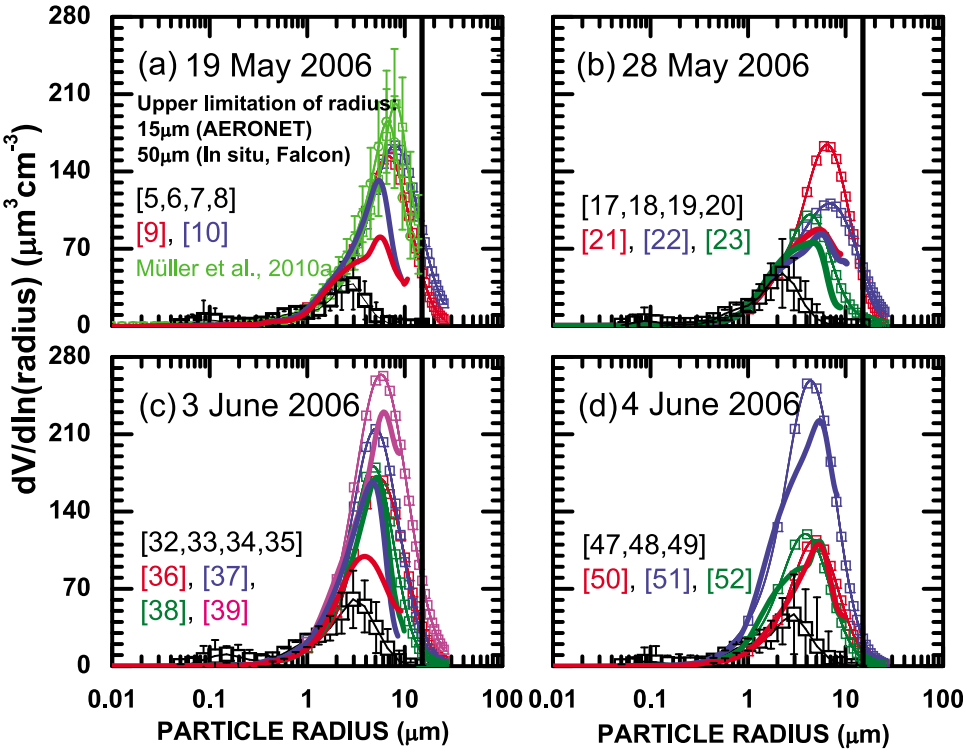

Figure 2. Particle volume size distributions (particle radius holds for volume-equivalent spherical particles) derived from AERONET Sun photometer measurements (black squares) and aircraft in situ measurements (colored lines). The results for Sun photometer are the average of several individual measurements. The numbers in brackets (black color) in each plot window refer to the individual measurements listed in Table 2. Regarding the airborne measurements we use the parameterizations of the size distributions in Table 4 of *Weinzierl et al.* [2009]. The numbers in color refer to the colored lines (blue, red, green, magenta), respectively, which then can be connected to Table 2 where we list the information on flight times and flight levels. The thin colored curves (with symbols) follow from the most reasonable assumption on the complex refractive index which is needed in the retrieval of the particle size distribution. The thick curves (without symbols) result from an extreme error analysis of the systematic uncertainty; details are given in the text. The green curves in Figure 2a also show the particle size distributions measured aboard Falcon on 19 May 2006 (same flight levels as for blue and red curves) [see *Müller et al.*, 2010a, Figure 1]. These size distributions were obtained with slightly different values of the parameterized lognormal particle size distributions. Vertical error bars denote one standard deviation.

the influence of variations of number concentration. Regardless of the scaling procedure that we carry out in the following, see section 3.2 and Figure 4, we see that the volume concentration of particles above 5 μm radius measured aboard the Falcon aircraft is on average larger than the particle volume concentration inferred by AERONET Sun photometer.

[42] The AERONET results do not show any particles with radius above 15 μm radius. This radius of 15 μm is the maximum particle size considered in the inversion of the AERONET optical data into particle volume size distributions.

[43] Regarding the measurement on 19 May 2006 we find that particle number concentration is less than 0.01 cm^{-3} in the radius range above 15 μm. We find similar concentrations for 28 May, 3 June and 4 June 2008 [see *Weinzierl et al.*, 2009, Figures 8 and 9]. The difference of the particle size distributions to the in situ measurements therefore cannot be explained by a significant concentration of particles above 15 μm radius.

[44] *Reid et al.* [2003, 2008] discuss in detail error sources that may lead to errors in particle size distribution measurements with aerodynamic and optical particle sizing instruments. Results impressively show significant variations of dust size distributions from North Africa and southwest Asia (Arabian Peninsula). In particular, optical measurement methods seem to be affected by uncertainties in data analysis.

[45] The cut point of the inlet and distribution system is particularly critical for measurements of mineral dust, as the concentration of coarse mode particles is naturally high. *Reid et al.* [2008] report on a value of 10 μm for the system they used for their observations. Thus there remains some uncertainty regarding the ability to fully resolve the coarse mode fraction of dust, as there are also uncertainties regarding the inlet efficiency. Regarding the Falcon observations we have to consider such uncertainties, too.

[46] We carried out an error analysis regarding the particle size distributions from Falcon. We wanted to test in how far a wrong assumption of the complex refractive index can

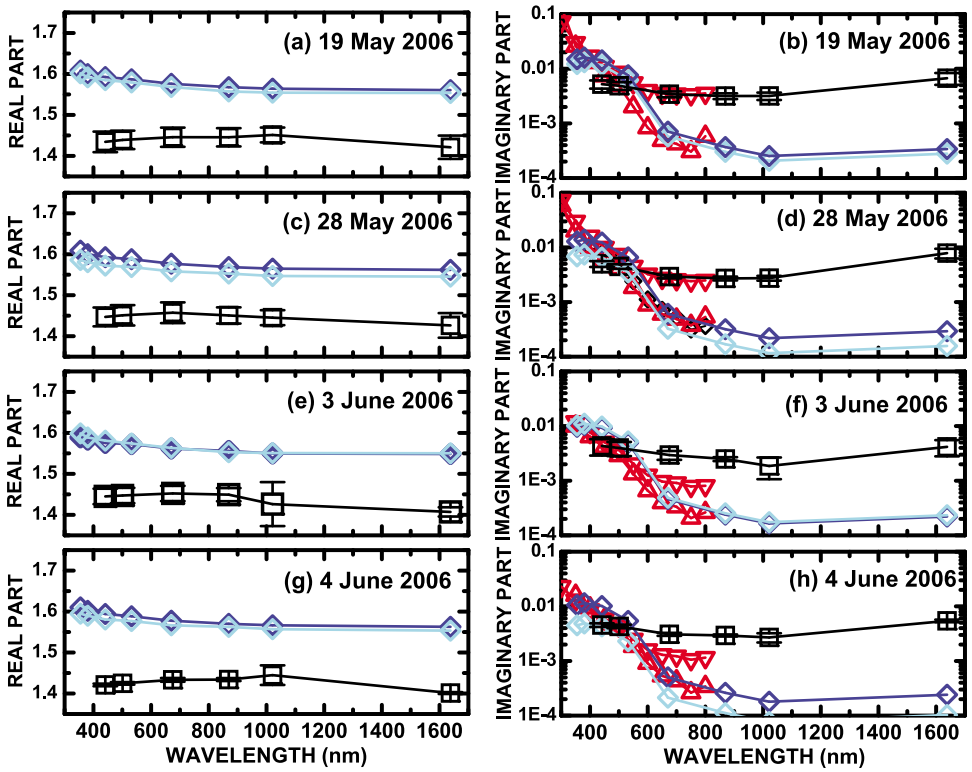

Figure 3. Mean complex refractive index determined from AERONET Sun photometer data (black symbols). The data represent the individual measurements, see Table 2: [5–8] for 19 May, [17–20] for 28 May, [32–35] for 3 June and [47–49] for 4 June 2006. Complex refractive indices were derived from analysis of the mineralogy of single particles collected aboard the Falcon aircraft (dark blue symbols) during flights over Ouarzazate on the four days [11, 12, 24–26, 40–42, 53, 54]. Complex refractive index was also derived from particles collected at Tinfou (light blue symbols) on these days. Imaginary parts (red symbols) were derived from observations of dust with SOAP at Tinfou. One set of numbers follows from the total absorption coefficients (downward pointing red triangles). The second set of numbers describes the contribution of pure dust (upward pointing red triangles). Details of the retrieval are given by *Müller et al.* [2009].

cause the significant systematic off-set between the size distributions from AERONET and from Falcon at particle radii above 3 μm. The complex refractive index is a necessary a-priori input parameter in the analysis of the data from the in situ particle sizing instruments. This value decides on the transformation from scattering signals, which is the primary data set of the particle sizing instruments, into particle size. A wrong value of the complex refractive index will result in wrong particle sizes and thus wrong particle size distributions. We varied the imaginary part of the complex refractive index between 0i and 0.004i. We think that these values determine the reasonable range of numbers that should be considered in signal analysis of the in situ particle sizing instruments.

[47] The result of our analysis is shown in Figure 2. The colored curves with symbols represent the particle size distributions with our best estimate of the complex refractive index (particularly the imaginary part). The thick colored curves (without symbols) represent the most extreme systematic offset. We assumed an imaginary part of 0i, i.e. non-absorbing dust, which is highly unlikely. We point out that the Falcon instrumentation included a PCASP (Passive Cavity Aerosol Spectrometer Probe) and several FSSPs (Forward Scattering Spectrometer Probe) for measurements of the coarse mode fraction. There is a radius range between approximately 0.5–3 μm diameter in which data from PCASP and FSSP are available [*Weinzierl et al.*, 2009]. Data analysis is considered successful if there is a match of the particle concentrations measured with PCASP and FSSP in this overlap region. This match can be achieved with a reasonable choice of the complex refractive index. We found that for certain choices of complex refractive indices we lose this agreement in the overlap region. In fact this mismatch can already be seen in the thick curves of Figure 2.

[48] In conclusion: Our main result of this analysis is that in fact the Falcon particle size distributions shift toward smaller particles, which brings them closer to the AERONET particle size distributions. Still, the overall discrepancy at particle radii above approximately 3 μm remains.

[49] Figure 3 shows the results for the real and imaginary part of the complex refractive index. This parameter was derived from the analysis of the mineralogy of single particles collected aboard the Falcon aircraft during flights over Ouarzazate. The complex refractive index was also derived from particles collected at Tinfou on these days. The complex refractive indices from the airborne data represent

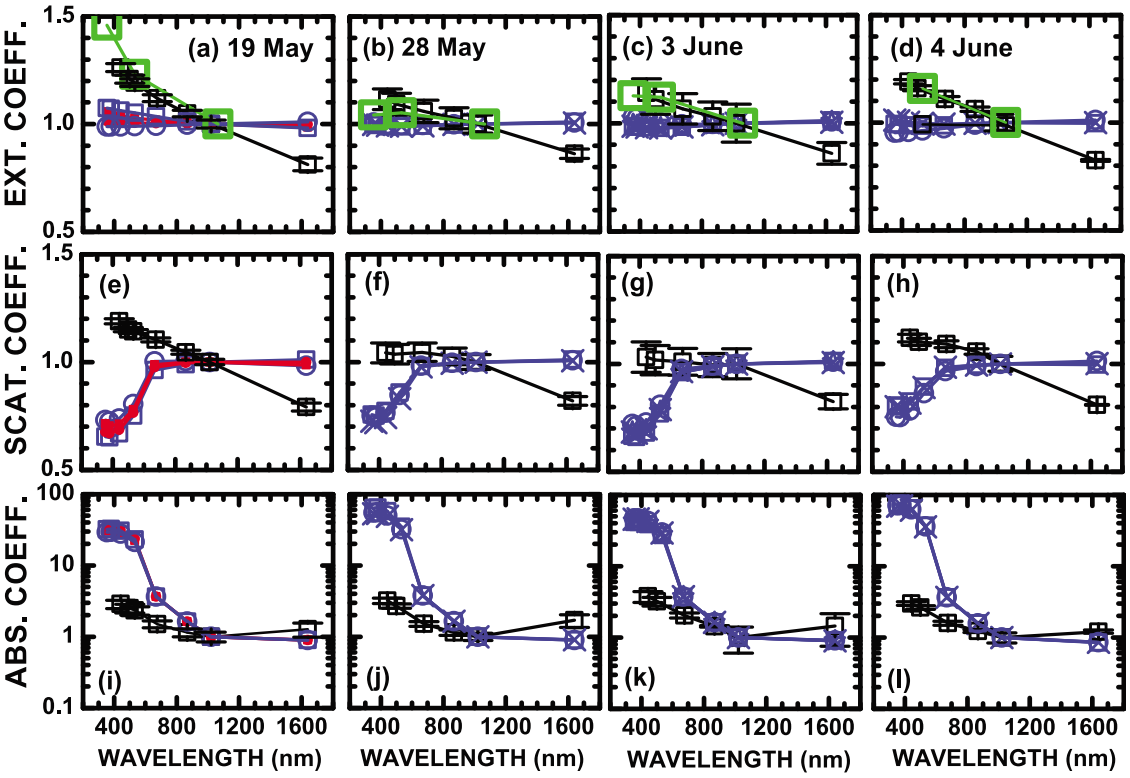

Figure 4. (a–d) Particle extinction, (e–h) particle scattering, and (i–l) particle absorption coefficients. Black symbols show the results from AERONET Sun photometer. The error bars (one standard deviation) describe the variability of the Sun photometer data. Green squares: Particle extinction coefficients were measured with POLIS at 355 nm [3, 15, 29] (data on 4 June [45] are of insufficient quality), with BERTHA at 532 nm [1, 13, 27, 43], and with MULIS at 532 nm [2, 14, 28, 44]; the numbers in brackets refer to the measurement times and days of Table 2. We use the combination of extinction data (at 532 nm) of both instruments (BERTHA and MULIS) in order to reduce the overlap height. The particle extinction coefficient at 1064 nm is estimated from measurements with HSRL [4, 16, 30, 31, 46]. Particle size distributions (see Figure 2) and complex refractive indices (see Figure 3) (from in situ measurements aboard the Falcon) were used for Mie-scattering computations. [9, 21, 36, 50] (blue squares), [10, 22, 37, 51] (blue circles), [23, 38, 52] (blue crosses), and [39] (blue stars; results for 3 June). The numbers denote the measurement times of the particle size distributions. Regarding the complex refractive index we used the mean value of [11, 12] for 19 May 2006, [24–26] for 28 May 2006, [40–42] for 3 June 2006, and [53, 54] for 4 June 2006. Results of Mie-scattering computations for the measurement on 19 May 2006 (red dots) are shown for comparison, see Figure 4 in *Müller et al.* [2010a].

particles with radius <1.25 μm. The ground-based results at the Tinfou site describe particles of radius as large as 250 μm.

[50] Imaginary parts were derived from observations of dust with an optical absorption spectrometer at Tinfou [*Müller et al.*, 2009]. We determined the imaginary part for the total absorption coefficient, and for the case in which we exclude the contribution of soot, i.e., we consider pure dust only. The mean values of the SOAP data in Figure 3 denote the most likely values. *Müller et al.* [2010a, Figure 4] show for the case of 19 May 2006 uncertainty bars. The uncertainty bars describe extreme values, i.e., maximum and minimum reasonable value. Details of the retrieval are given by *Müller et al.* [2009]. The uncertainty bars for the results of 28 May and 3/4 June 2006 do not differ in a significant way from the uncertainty bars we obtained for the results on 19 May 2006.

[51] The results for the measurement on 28 May and 3/4 June 2006 are similar to the findings for 19 May 2006 [*Müller et al.*, 2010a]. The real parts from AERONET retrievals are lower than the real parts from the airborne in situ observations. We find at minimum 0.1 lower values for the real part from the Sun photometer to real part from the in situ data. This minimum deviation mainly occurs in the wavelength range between 869 to 1021 nm. Deviations increase to 0.13–0.15 at 441 nm which is the shortest measurement wavelength of the AERONET instrument. We also find an increasing deviation of 0.12–0.16 between AERONET Sun photometer and in situ based real parts at 1638 nm. However, as we pointed out in the methodology section (section 2), the calibration of the Sun photometer channel at 1638 generally is worse than the calibration at the other wavelengths. Thus, this increasing deviation in the infrared region cannot be taken as final conclusion on the

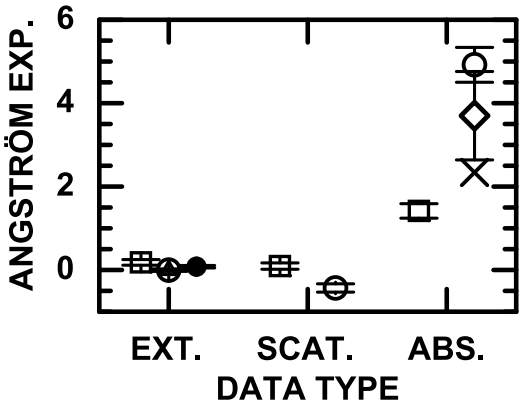

Figure 5. (EXT.) Particle extinction-related Ångström exponents, (SCAT.) particle scattering-related Ångström exponents, and (ABS.) particle absorption-related Ångström exponents derived from AERONET Sun photometer measurements (black squares) and computed from particle size distributions and complex refractive indices (circles). We computed the Ångström exponents for the wavelength pair 441/869 nm from the data shown in Figure 4. Also shown is the extinction-related Ångström exponent from lidar (bullets). It has been computed for the wavelength pair 355/532 nm. We reanalyzed data on the basis of nephelometer and PSAP measurements for the absorption-related Ångström exponents (diamond). Details are explained in the text. We also show results from PRIDE (cross) [*Bergstrom et al.*, 2007]. Error bars denote one standard deviation.

accuracy of the retrieval of the real parts with Sun photometer data.

[52] Regarding the imaginary part we also find differences. The differences are particularly large at the short measurement wavelengths. At 441 nm AERONET Sun photometer results are 0.0002–0.009 lower than the airborne results. This deviation is equivalent to 5% lower imaginary parts on 4 June and 63% lower values on 28 May 2006.

3.2. Shape-Independent Optical Parameters

[53] Figure 4 shows the column-mean extinction coefficients inferred from optical depth measured with AERONET Sun photometer. We determined the dust layer height from the range-corrected lidar backscatter signals taken during or shortly after the Sun photometer observations. Furthermore we scaled our data to particle extinction at 1064 nm. This normalization is of advantage as we avoid in this way the effect of inhomogeneities of the number concentration in the dust plumes. This is particulary important for the comparison with the airborne results.

[54] We find good agreement to mean extinction coefficients from the ground-based Raman lidar observations (POLIS, BERTHA, and MULIS) at 532 nm. The deviations are larger at 355 nm.

[55] Figure 4 also shows extinction coefficients derived from airborne HSRL observations at 1064 nm. We assumed lidar ratios of around 55 sr in the retrieval [see also *Tesche et al.*, 2009; *Müller et al.*, 2010a]. Naturally, due to our scaling, particle extinction agrees to particle extinction from Sun photometer. If we compare the absolute values (not shown) we also find good agreement of the mean extinction from HSRL to mean extinction from the AERONET instrument.

[56] We derived the particle extinction coefficients from light-absorption coefficients measured with the 3-wavelength PSAP (467, 530, and 660 nm) aboard the Falcon aircraft and particle scattering coefficients which were derived from nephelometer observations. Details on how this was done are given by *Petzold et al.* [2009] and *Weinzierl et al.* [2009]. A summary of the main steps is given by *Müller et al.* [2010a].

[57] We also derived extinction coefficients from Mie-scattering computations [*Weinzierl et al.*, 2009]. We used airborne measurements of particle size distributions [see *Weinzierl et al.*, 2009, Table 4] and complex refractive indices as input information for the computations.

[58] *Müller et al.* [2010a, Figure 6] show the comparison of extinction coefficients at the three wavelengths of the nephelometer/PSAP method and the Mie-scattering computations for the measurement of 19 May 2006. We find reasonable agreement of the two data sets. Particle extinction coefficients were inferred with the nephelometer/PSAP method at 530 nm for the measurements on 28 May and 4 June 2006. *Weinzierl et al.* [2009, Table 4] provides us with the necessary information. There is reasonable agreement in magnitude of the measured extinction coefficients to the Mie-scattering computations at 530 nm, but disagreement in the wavelength dependence, particularly between the UV and near-IR.

[59] For this reason we only show results of Mie-scattering computations using particle size distributions for the following discussion. We computed the extinction coefficients for the wavelength range from 350 nm to 1638 nm. We scaled (normalized) our results to the extinction coefficient at 1064 nm.

[60] We find in general a rather flat extinction spectrum, i.e., particle extinction does not change significantly with wavelength. This result has to be expected in view of the large particles that were measured aboard the Falcon aircraft. The spectral slope of particle extinction is different from the spectral slope measured by lidar and Sun photometer. The absolute values of particle extinction (not shown) from the Mie-scattering computations are larger than what was measured by lidar and Sun photometer [see also *Müller et al.*, 2010a, Figure 6; *Weinzierl et al.*, 2009, Figure 12].

[61] There may be several reasons for the discrepancies between lidar/Sun photometer data and the aircraft data. We tested in various ways [*Müller et al.*, 2010a] if deviations of the extinction coefficients are caused by the time gap in observation times, or the fact that 1) lidar delivers vertically resolved extinction coefficients (which can be converted to column-mean values), 2) Sun photometer observations provide optical depth (which subsequently can be converted into column-mean extinction coefficients if dust layer height from lidar observations is taken), and 3) airborne measurement describe particle extinction coefficients in various flight levels. We conclude that like in the case of the measurement of 19 May 2006, dust plume inhomogeneities cannot be the main cause of the discrepancy.

[62] Regarding the Mie-scattering computations it is clear that there are approximation errors in our computations, because dust particles are not spherical in shape. It is impossible to assess the exact approximation errors but we

may estimate this error on the basis of our extinction measurements. If we use the results of Figure 4 we see that approximation errors may be as large as 25% at 532 nm; see measurement on 19 May 2006. The minimum deviation is 10% at 532 nm; see measurement on 28 May 2006.

[63] We carried out computations of particle extinction for the case of 19 May 2006, assuming in one case spherical particle shape and in another case spheroids. In both cases we used the same particle size distributions. We find a 10 %-deviation for the extinction coefficients. 10% approximation error, however, also cannot explain for the deviation of the Falcon data to the remote sensing data. More importantly, the extinction values are larger (if we look at the absolute numbers) when we use spheroids in our computations. The spectral slope did not change significantly, either.

[64] The discrepancy of extinction coefficients from airborne data to extinction coefficients from lidar and Sun photometer increases with increasing measurement wavelength, which is particularly obvious if we look at the absolute values (not shown in the plots). The accuracy of optical depth measurements with Sun photometer is high. Measurement errors therefore cannot account for the observed differences. A wrong assumption of dust layer height, which serves as scaling factor for converting optical depth into extinction coefficients cannot explain the discrepancies either.

[65] Uncertainties of the parameterizations of the measured particle size distributions can be one reason for the discrepancies. We used the parameterizations of the measured particle size distributions as given in Table 4 of *Weinzierl et al.* [2009]. The rather low wavelength dependence of the particle extinction coefficients requires a considerably high share of large particles. However, we emphasize once more: the Sun photometer optical depth measurements are very accurate. We see a non-negligible wavelength dependence, which indicates that there may not be such a strong contribution of coarse mode particles, as suggested by the in situ measurements.

[66] Figure 4 also shows particle scattering and absorption coefficients. A detailed discussion is given by *Müller et al.* [2010a] for the measurement of 19 May 2006. In that contribution we already noted the large differences between the scattering coefficients derived from the AERONET and the airborne in situ data. Figure 4 shows once more the scattering coefficients from Figure 6 of *Müller et al.* [2010a]. Our new results for 28 May, and for 3 and 4 June 2006 corroborate the findings for 19 May 2006. With decreasing wavelength there is increasing difference between scattering inferred from the AERONET data to the scattering coefficients inferred with Mie-scattering computations from the aircraft data.

[67] We also find increasing differences of the absorption coefficients from AERONET Sun photometer and Falcon aircraft data for all four measurement days. The discrepancies increase with decreasing measurement wavelength. We consider it unlikely that the shape assumption in the computations, i.e., spherical particles rather than spheroids can fully account for the discrepancies. We need to keep in mind that we use a wavelength-dependent complex refractive index in the light-scattering computations. Any error in this wavelength-dependence transfers into errors of the wavelength-dependent absorption coefficient. As we can see from Figure 3 there is a significant difference of this wavelength-dependent imaginary part of the complex refractive index between the AERONET data and the Falcon data. Another error source could be that our methods in general only provide an effective complex refractive index. This effective value could depend on the measurement method, which means that the absorption coefficient might depend on the measurement method.

[68] Figure 5 summarizes our results for the optical data in terms of the Ångström exponents. We computed the Ångström exponents from the Sun photometer, lidar, and in situ measurements, respectively, for the visible wavelength range. Extinction-related values from lidar agree to the AERONET results. We find 0–0.2 for the extinction-related Ångström exponent. This range describes the mean condition on all four measurement days for the wavelength pair 441/869 nm (AERONET Sun photometer) respectively the wavelength pair 355/532 nm (lidar). The airborne results also show good agreement to the Sun photometer data. The airborne measurements cover the wavelength range from 441 to 869 nm.

[69] The choice of the wavelength pairs is important for the Ångström exponents. We can infer scattering and absorption coefficients from AERONET data and from Mie-scattering computations of the airborne in situ data, but not from lidar. We find a slight discrepancy for the scattering-related Ångström exponent at all wavelengths below 700 nm.

[70] With respect to the absorption-related Ångström exponent the differences are significant; see also *Müller et al.* [2010a]. Figures 4i–4l show that the absorption coefficients from Sun photometer and the airborne observations differ significantly at the wavelengths below approximately 700 nm.

[71] The Mie-scattering computations of the absorption coefficients result in absorption-related Ångström exponents of approximately 4.5–5.5 (wavelength pair 441/869 nm). These values are considerably larger than the value of approximately 1.5 that we find from the AERONET data. The values from our Mie-scattering computations are anomalously higher than absorption-related Ångström exponents published in literature. *Bergstrom et al.* [2007] and *Russell et al.* [2010] report on values of 2.34 for Saharan dust observed in the far-field of the North African source region. The measurements were carried out during PRIDE in the Caribbean Sea [*Reid et al.*, 2003]. *Coen et al.* [2004] report on values as high as 2 derived from absorption measurements of Saharan dust observed at the high-altitude station Jungfraujoch in Switzerland. *Fialho et al.* [2005] report on values of 2.9 for Saharan dust.

[72] Figure 4 shows only the results of Mie-scattering computations in which we use the airborne particle size distribution measurements and the complex refractive index found by *Kandler et al.* [2009]; see Figure 3. This choice of the complex refractive index to our opinion may deliver a reasonable maximum value of the absorption coefficients across the wavelength range considered in our study. Particularly the strong wavelength-dependence of the imaginary part, i.e. the strong increase of this parameter toward shorter wavelengths may be responsible for the unusually strong increase of the light-absorption coefficient with decreasing wavelength, i.e., from around 700 nm down to 441 nm. Note that the results of the optical properties in which we use the

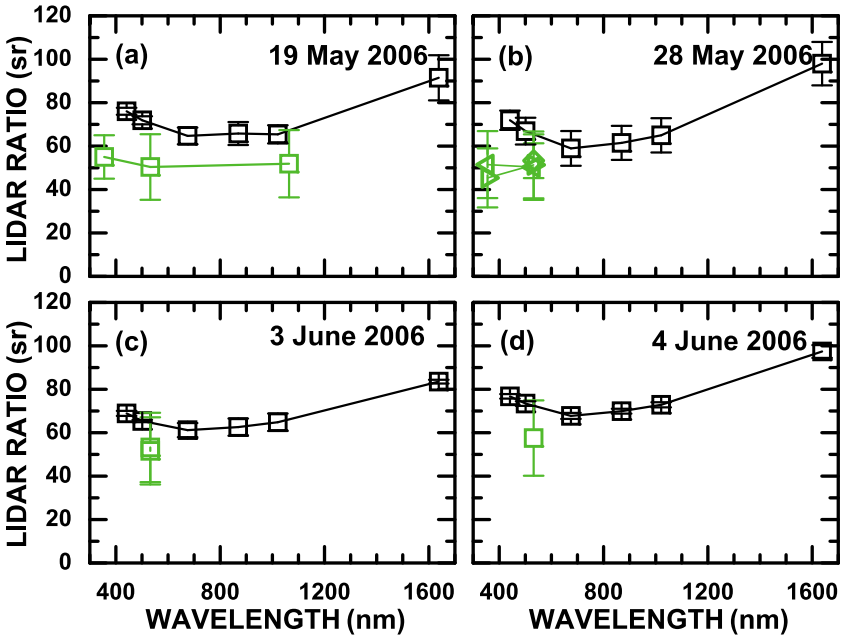

Figure 6. Particle lidar ratios measured with lidar (green) and computed from AERONET data products (black). The computations are described by *Müller et al.* [2010b]. The lidar data are from POLIS (355 nm), MULIS (532 nm), and HSRL (1064 nm). The data describe averages and are computed from the different lidar instruments and Sun photometer according to the measurement times listed in Table 2.

nephelometer and PSAP data is shown for 19 May 2006 in Figures 4a, 4e, and 4i. We do not believe that the choice of the wavelength range that has been used for the computations of the absorption-related Ångström exponent can fully account for the considerably larger values we find in our study.

[73] In order to find a lower limit of the absorption coefficient and particulary a lower reasonable value of the absorption-related Ångström exponent we carried out another sensitivity study in which we tried to extract the effect of an incorrectly chosen complex refractive index in our data analysis. For this purpose we once more analyzed our airborne data of nephelometer and PSAP measurements of dust scattering and absorption properties according to the scheme described by *Petzold et al.* [2009] and *Weinzierl et al.* [2009]. We modified however our assumption on the imaginary part in this scheme in such a way that we considered lower imaginary parts.

[74] We find a mean value of 3.7, see Figure 5. The variability, expressed in terms of standard deviation is 1.1. The lowest value from an individual measurement is 2.6 ± 0.16 (Falcon measurement on 3 June 2006, flight leg L04; see Table 2), the largest value is 5.3 ± 1.4 (Falcon measurement on 4 June 2006, flight legs L03 and L04). Only the lowest individual measurement value that we used for computing the mean value of all 4 comparison days is in the upper range of numbers reported by *Bergstrom et al.* [2007] and *Russell et al.* [2010].

[75] We can merely speculate on the possible reasons for the differences between our results and the numbers reported in the literature. We measured pure Saharan dust from a specific source region in North Africa during SAMUM 2006, whereas the location of the source regions in the other publications was less well defined. Particles observed in SAMUM were on average larger than what has been reported by *Reid et al.* [2003] for PRIDE which focused on mineral dust in the far field of the North African dust sources. We do not know if smaller dust particles may lead to smaller absorption-related Ångström exponents. We do not know if different measurement techniques used for measuring the same parameter, i.e., the particle light-absorption, can lead to different absorption-related Ångström exponents.

[76] In other words: we have insufficient information to decide if remote sensing methods that infer the absorption coefficient and its spectral dependence inherently deliver results different from in situ observations of the light-absorption coefficient, regardless of measurement errors. We need to keep in mind that the light-absorbing components are not evenly distributed in dust grains. Thus, there is the question, if this spatial distribution in dust may have an effect on the overall light-absorption capacity at various wavelengths, and we do not know in how far the various measurement methods are sensitive regarding this spatial inhomogeneity.

3.3. Shape-Dependent Optical Parameters

[77] In another step we use the AERONET data to compute particle parameters that depend strongly on particle shape, i.e., extinction-to-backscatter (lidar) ratios and linear particle depolarization ratios. These parameters are measured directly with lidar without knowledge of particle shape.

[78] This part of our study is particularly important for our goal of using the AERONET light-scattering model for our lidar data inversion methodology [*Müller et al.*, 1999a, 1999b]. The equations that are used for the computations of these two parameters are presented by *Müller et al.* [2010b].

[79] Figures 6 and 7 show the results for particle lidar ratio and linear particle depolarization ratio, respectively. Because

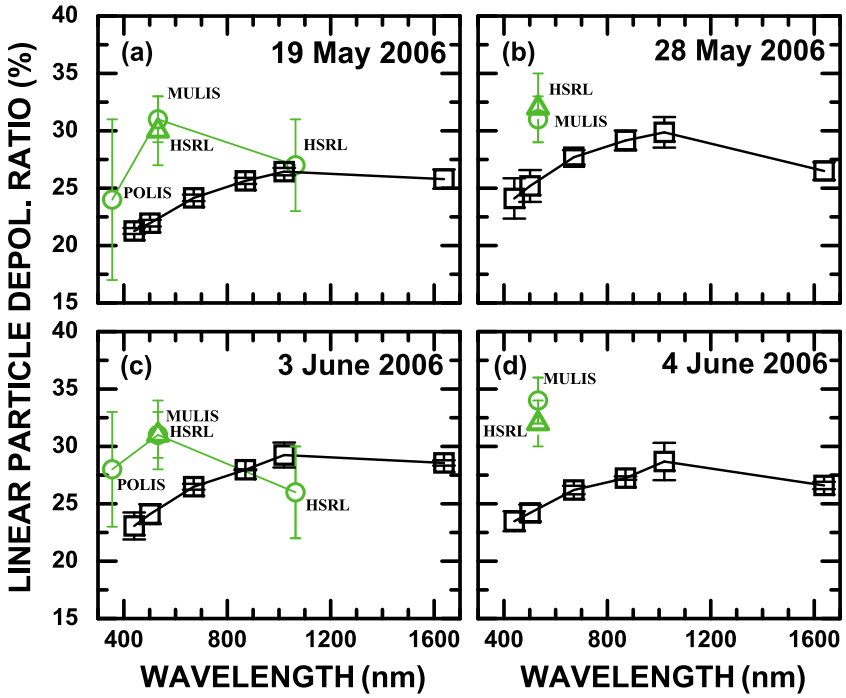

Figure 7. Linear particle depolarization ratio measured at 355 nm (green circle; POLIS), 532 nm (green circle (MULIS) and green triangle (HSRL)), and 1064 nm (green circle; HSRL). Shown are the results for (a) 19 May [2–4] in Table 2, (b) 28 May 2006 [14, 16], (c) 3 June [27–31], and (d) 4 June 2006 [44, 46]. Error bars denote the systematic uncertainty [see *Freudenthaler et al.*, 2009, Table 2]. Column-mean linear particle depolarization ratios were calculated from Sun photometer data at 441, 501, 675, 869, 1021, and 1638 nm. The equation used for the computations is given by *Müller et al.* [2010b]. We used the Sun photometer measurement times listed in Table 2. We computed mean values for each day. Error bars denote one standard deviation.

of the complexity of the lidar measurements we did not obtain the complete set of these two parameters for all four measurement days.

[80] We find reasonable agreement for the lidar ratio at 532 nm. Discrepancies are particularly obvious at 355 nm. The numbers from Sun photometer are significantly larger. We cannot measure with lidar the lidar ratio at 1064 nm. We estimated this value [*Tesche et al.*, 2009].

[81] We compare our results to a study carried out with AERONET Sun photometer data [*Cattrall et al.*, 2005]. The authors present lidar ratios derived from AERONET Sun photometer observations in various regions on the globe. One set of results in this study deals with mineral dust. The authors infer values of approximately 35 sr for the site of Banizoumbou (Nigeria) and 38 sr for Capo Verde (Sal Island, Cape Verde Islands). As in this present study, the particle backscatter coefficient had to be computed from the AERONET data products of particle size distribution and complex refractive index. Errors in the computation of the backscatter coefficients with the AERONET dust light-scattering model may be responsible for the lower lidar ratios compared to the lidar ratios we obtained from SAMUM; see also the discussion in section 4 of *Müller et al.* [2007]. Aside from this error source another source of uncertainty again is the fact that Sun photometer measures aerosols in the atmospheric column. Dust over Banizoumbou may experience some impact from continental particles. Dust over Capo Verde may be affected with marine particles.

[82] With respect to the linear particle depolarization ratio we find 20%–30% higher values from lidar compared to the Sun photometer data in the visible wavelength range (500– 550 nm). There is good agreement between lidar and Sun photometer data at 1064 nm.

[83] We have few data on depolarization ratios. Though the lidar data underwent careful quality control there still remains a lot of uncertainty regarding the spectral slope of the linear particle depolarization ratio. SAMUM 2008 was carried out in the Republic of the Cape Verde in 2008 [*Ansmann et al.*, 2011]. This field campaign will provide us with particle depolarization ratios of higher quality. We shall analyze these data in a future contribution.

4. Statistical Analysis

[84] In the previous section we discussed in detail the results of four measurement days for which we have a nearly complete set of data from several measurement platforms. The data were taken comparably close to each other in terms of distance and in terms of temporal off-set between measurement times of each measurement platform, respectively. In the next step we analyzed the complete measurement period, which thus offers us a more statistical view on the inferred data products. We do not compare the data on a day by day basis as we do not have aircraft observations at Ouarzazate on more than a few days. Intensive dust optical and microphysical properties varied comparably little among

Table 3. Measurement Days and Number of Data Sets From the Various Instrument and Measurement Methods That Were Used for the Statistical Analysis of the Data Products Discussed in Section 4[a]

	AERONET		Lidar, Ground		Falcon		Tinfou, Ground	
Parameters	Measurement Days	Number of Samples	Measurement Days	Number of Samples	Measurement Days	Number of Samples	Measurement Days	Number of Samples
psd	24	60	-	-	6	36	-	-
cri, real (441)	24	54	-	-	6	6	15	15
cri, real (532)	24	57	-	-	6	6	15	15
cri, real (1021)	24	62	-	-	6	6	15	15
cri, imag (441)	24	54	-		6	6	15	15
cri, imag (532)	24	57	-	-	6	6	15	15
cri, imag (1021)	24	62	-	-	6	6	15	15
lr (355)	24	38	15	17	-	-	-	-
lr (532)	24	39	19	24	-	-	-	-
lr (1064)	24	47	-	-	-	-	-	-
depol (355)	24	53	2	2	-	-	-	-
depol (532)	24	53	20	25	5	5	-	-
depol (1064)	24	60	-	3	5	3	-	-
ssa (350)	24	48	-	-	-	-	26	26
ssa (450)	24	48	-	-	-	-	26	26
ssa (550)	24	48	-	-	-	-	26	26

[a]Particle number distribution is denoted by psd. Complex refractive index is denoted by cri. Depol. denotes the linear particle depolarization ratio of dust. The single-scattering albedo is denoted by ssa. Numbers in brackets denote the measurement (retrieval) wavelength in nm. Regarding the linear particle depolarization ratio at 532 nm, we only use the results from MULIS [see *Freudenthaler et al.*, 2009, Table 2]. Results from the airborne HSRL are listed for 532 nm and 1064 nm in Table 2 of *Freudenthaler et al.* [2009]. Here, we only include the results at 1064 nm.

the different measurement days, see the SAMUM 2006 special issue in TELLUS, 61 B (2009). Table 3 lists the number of observation days and the number of individual data sets that we use for our statistical analysis. We point out that for some of the parameters we have more samples than measurement days from AERONET, lidar and Falcon measurements. These data sets (number of samples taken) in large part describe independent measurements, as they were done at different times (AERONET) or different flight levels (Falcon). In the case of lidar there are a few cases in which we split measurements on specific days into two intervals, as the aerosol conditions notably changed during the measurement time.

4.1. Microphysical Parameters

[85] Figure 8 shows the mean particle size distribution inferred from AERONET Sun photometer on 24 days. Also shown is the mean particle size distribution inferred from the airborne measurements on 6 days on which the aircraft flew over Ouarzazate. Particle effective radius of the coarse mode fraction of mineral dust observed with the AERONET Sun photometer is a factor two lower compared to effective radius inferred by the airborne observations carried out in different flight levels on the different flight days [see *Weinzierl et al.*, 2009; *Müller et al.*, 2010a].

[86] *Reid et al.* [2003] report on considerable variation of dust particle size distributions measured during PRIDE. The dust was observed with ground-based impactors (MOUDI and DRUM) and aerodynamic particle sizers (TSI aerodynamic particle sizer), and airborne PMS (Particle Measuring Systems) FSSP-100 and PCASP-100X. One conclusion of the comparison of the particle size distributions measured with the in situ instruments was that the different measurement techniques may be accountable for the observed variations. The aerodynamic particle sizer used in that study was considered the most reliable instrument for particle sizing. In contrast, the airborne FSSP-100 consistently oversized particles by more than a factor two [*Reid et al.*, 2003]. Reasons for the oversizing were low responses to particles in the diameter range from 3 – 10 μm, insufficient knowledge of the complex refractive index which is needed

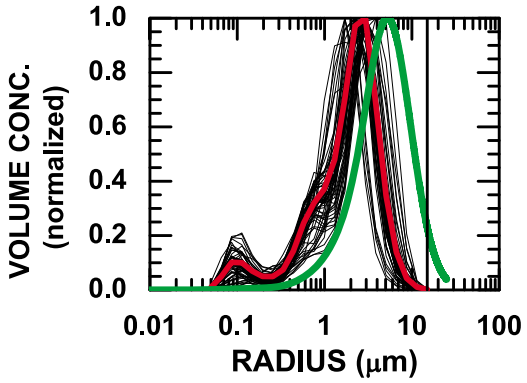

Figure 8. Mean particle size distribution (red) inferred from AERONET observations. The particle size distribution represents the mean value of 60 individual size distributions (black lines); see Table 3. The particle size distribution includes only data for which the Ångström exponent for the wavelength pair 501/1021 nm was less than 0.4 [see *Tesche et al.*, 2009, Figure 4] and the Ångström exponent for the wavelength pair 379/501 nm was less than 0.7. For that reason we excluded the measurement days of 11/12 May 2006 and 29 May to 1 June 2006. We furthermore excluded 4 observations for which we could not clearly distinguish the fine mode from the coarse mode fraction of the size distribution. Also shown is the mean particle size distribution (green) measured aboard the Falcon aircraft during overflights over Ouarzazate. We averaged 11 individual size distributions. The black vertical line denotes the cutoff radius of the Sun photometer inversion scheme.

for particle sizing, and the fact that particles are not spherical.

[87] *Reid et al.* [2003, Table 1] summarize results for volume median diameters of Saharan dust. The data represent observations over Niger (West Africa), Tenerife (Canary Islands in the North Atlantic off the west coast of Morocco), the Cape Verde Islands (in the tropical North Atlantic Ocean off the coast of Senegal), and Puerto Rico (Caribbean Sea). The first place is close to one of the North African dust sources, i.e., the Bodélé Depression in Chad. Tenerife and the Cape Verde Islands are still close to the North African source of dust. Puerto Rico is in the far-field of Saharan dust. *Reid et al.* [2003] report on significant variations of particle size. Regarding the first three sites volume median diameters (optical equivalent) are >6 μm (Niger), >8 μm (Tenerife), and 13 $\pm$ 2 μm (Cape Verde Islands). Regarding the far-field site (Puerto Rico) the authors find a volume median diameter of 9 $\pm$ 1 μm.

[88] A summary on desert dust observations with Sun photometers shows that optical inversion methods result in volume median diameters of 3–7 μm [see *Reid et al.*, 2003, Table 1]. Various Saharan dust regions are considered.

[89] In view of the critical discussion given by *Reid et al.* [2003] on measurement accuracies of various particle sizing methods there remains the question if the variations in particle size are due to differences in Saharan dust regions, transport times and distances (compare Cape Verde results with those at Puerto Rico), or the applied measurement methods.

[90] *Reid et al.* [2003] also report on volume median diameters of desert dust observed during PRIDE. Values are 3.6 μm (geometric diameter). The data were obtained from measurements with APS (Aerodynamic Particle Sizer). APS provides in the first step an aerodynamic volume diameter which subsequently can be transferred into a geometric median value. For details on how this was done we refer to *Reid et al.* [2003]. *Reid et al.* [2003, Figure 9] furthermore give an impression on the uncertainties of the computations. It is interesting to note that there appears to be a secondary peak in the volume size distribution which could shift the geometric median diameter toward larger values of 6.5 μm, though this option was ruled out by *Reid et al.* [2003].

[91] Saharan dust was observed during the United Arab Emirates Unified Aerosol Experiment (UAE^2) [*Reid et al.*, 2008]. Measurements were carried out at an Arabian Gulf coastal site which experienced dust from several sources within southwest Asia. Among the instruments were aerodynamic particle sizer, a DRUM cascade impactor, and an AERONET Sun photometer. As in the case of the PRIDE campaign the authors report on volume median diameters of approximately 3.5 μm and a standard deviation of 30%. The median diameter ranges from 3.25–4.56 μm in dependence of dust source region identified in this field experiment [see *Reid et al.*, 2008, Table 1]. AERONET Sun/sky retrieval resulted in volume median diameters (optical equivalent) of 4.1–6 μm.

[92] Regarding the AERONET Sun/sky inversions we find volume median diameters between 2.96–8.86 μm for the SAMUM 2006 data set. The mean value is 4.37 $\pm$ 0.95; we only report the radius for the coarse mode fraction. Regarding the Falcon in situ measurements, *Weinzierl et al.* [2009] find a volume median diameter of 15.5 $\pm$ 10.9 μm, mean values range from 8–18 μm, except for some outliers [see *Weinzierl et al.*, 2009, Figure 13]. This range of numbers is considerably larger than the diameters from the AERONET measurements and the values reported by *Reid et al.* [2003, 2008], except for the Cape Verde field site (13 $\pm$ 3 μm). We can only speculate on the reasons for the discrepancy.

[93] On the one hand measurement errors of the instruments operated aboard the Falcon aircraft may be responsible, aside from the possibility that each of the field sites (in Niger, Tenerife, Cape Verde Islands, Puerto Rico, Arabian Gulf region) may have been affected by dust emitted from different source regions. On the other hand, *Weinzierl et al.* [2009] point out in their discussion of the airborne dust size measurements that the particle number concentrations measured with the FSSP-300 and the PCASP-100X showed close agreement in the particle size region were both instruments measure. This latter argument may serve as argument that the FSSP observations which largely decide on our finding of discrepancy between AERONET and airborne in situ observations may not be the primary cause of the discrepancies. We must keep in mind that SAMUM 2006 was a field campaign in which we obtained comparably strong instrument signals due to the proximity of our instrument platforms to the source region. In contrast, PRIDE may be considered as a representative site for the far-field region. It is still unclear what may happen to dust size distributions along their journey of several thousand kilometers across the Atlantic Ocean. However, UAE^2 was also located in a region of strong dust emissions, still particle size distributions also result in considerable smaller median volume diameters compared to the results inferred from the Falcon observations; the inlet cutoff diameter was at 10 μm.

[94] Figure 8 shows that there is a small fraction of particles in the size range around 100 nm in radius. We believe that this fine mode fraction may not necessarily be a retrieval error, but a real feature of the mean particle size distribution. We need to keep in mind that the field site is located in the Draa Valley which is a comparably densely populated region. There is a significant amount of car traffic, and emissions from trucks. There are plenty of agricultural activities, and the burning of agricultural waste is quite common in this area. Thus there is the possibility that small particles may be present in the atmospheric column. The airborne measurements do not cover the lowest few hundred meters of the atmospheric column, and thus it is not possible for us to verify this small mode fraction by the airborne measurements at Ouarzazate.

[95] Figure 9 presents a comparison of the wavelength dependence of the real and imaginary parts that are derived from the AERONET data and from the mineralogical analysis of the ground-based particle measurements at Tinfou. The airborne observations of particle complex refractive index do not differ significantly from the observations at Tinfou [*Kandler et al.*, 2009].

[96] The in situ measurements show that the real part is nearly independent of the measurement wavelength. The technique of determining the refractive index from mineralogy is based on fixed values for pure minerals, which have mostly very similar refractive indices and are known with high accuracy. The variability reflects only changes in

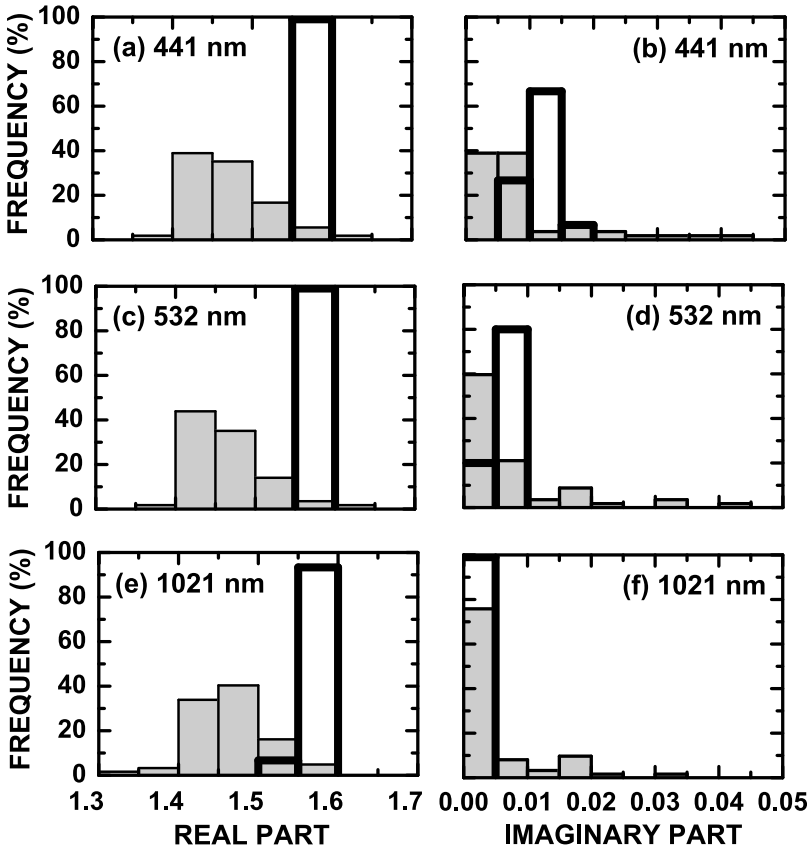

Figure 9. Frequency distributions of the real part and imaginary part of the complex refractive index determined from AERONET Sun photometer data (grey columns) and from mineralogical analysis of particles collected at the ground at Tinfou (open columns). Results are shown for the wavelengths at (a, b) 441 nm, (c, d) 532 nm, and (e, f) 1021 nm. Results of the Tinfou data do not differ in a significant way from the results of airborne sampling. The results are the mean values. The number of individual measurements used for this comparison is listed in Table 3.

composition. The standard deviation of the real part that follows from the available time series at Tinfou [*Kandler et al.*, 2009] is between 0.004 and 0.012 (relative standard deviation of 0.3% to 0.8%), depending on wavelength and particle size. Including an additional potential variability in silicate composition, which cannot be identified by our single particle analysis, we estimate an uncertainty of 0.03 for these refractive index values.

[97] The imaginary part increases with decreasing wavelength, and we obtain significantly larger values at near ultraviolet wavelengths. The frequency distribution (describing the three wavelengths at 441, 532, and 1021 nm) shows that the overall variability of the imaginary part was rather low during the measurement period.

[98] The uncertainty in imaginary part that is derived from the mineralogical analysis is considerably higher, reflecting our poor knowledge on basic mineral absorption and the uncertainties of the mixing rules, as well as the influence of minor compounds (mainly iron compounds) inside single particles. At Tinfou, a relative standard deviation between 20% and 50% has been found. Including the mentioned uncertainties in the base data, the total uncertainty in the imaginary part is a factor of 2 for dust particles. For a more detailed discussion we refer to *Kandler et al.* [2011].

[99] *Petzold et al.* [2009, Table 3] report on mean real and imaginary parts for different dust episodes. The results were derived from measurements of particle size distributions and PSAP observations aboard the Falcon aircraft. Mean values of the real part are between 1.546 and 1.565 for the wavelengths 450, 550 and 700 nm, which is close to the values reported from the mineralogical analysis. Mean imaginary parts vary between 0.0031–0.0052 at 450 nm and between 0.0003–0.0025 at 700 nm. These numbers are lower than what we obtain from the mineralogical analysis. The uncertainty is approximately $\pm 25\%$. We note that these numbers describe only particles with diameter below 2.5 μm.

[100] The Sun photometer observations show a comparably weak wavelength dependence of the real part. The variation of the values at the three wavelengths is broader compared to the values inferred from the in situ data (mineralogical analysis). This scatter may be caused by measurement errors of the optical input data that are used for data inversion.

[101] Measurement errors may result from calibration errors. We cannot exclude that dust optical properties varied stronger during the complete period of SAMUM 2006 than what was measured during the comparably few overflight days of the Falcon aircraft. These changes of optical properties may either be caused by changes of the particle size

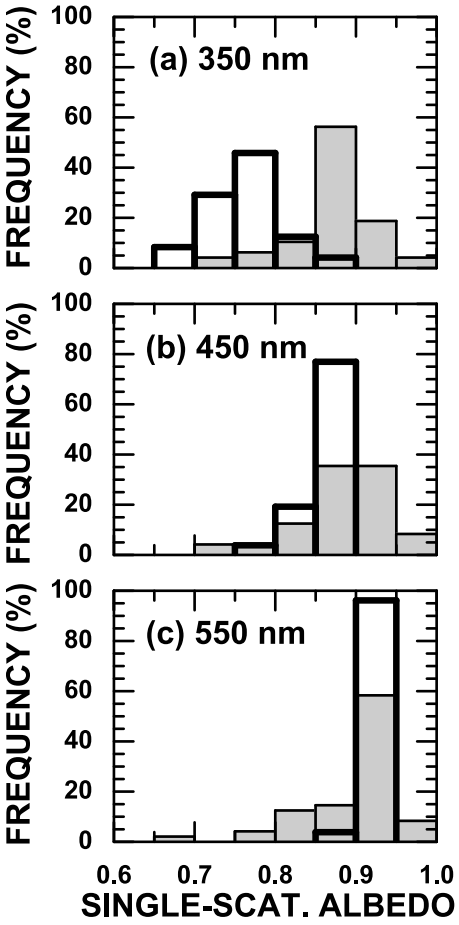

Figure 10. Frequency distributions of single-scattering albedo at (a) 350 nm, (b) 450 nm, and (c) 550 nm. Results are shown for AERONET Sun photometer (grey columns) and for SOAP measurements (open columns). The results represent the number of samples listed in Table 3.

distribution or changes in chemical composition. Uncertainties of the inversion procedure may be responsible for a larger scatter of the results, too.

[102] Regarding the imaginary part we see that particle-light absorption increases with decreasing measurement wavelength. Similarly to the real part, the absolute values of the imaginary part are different from the values that we obtain with our in situ measurement technique. On average, we find lower imaginary parts at the shorter wavelengths compared to the imaginary parts that follow from the in situ particle analysis.

4.2. Optical Parameters

[103] One important parameter derived from the SAMUM 2006 campaign is single-scattering albedo. Figure 10 shows the results. *Müller et al.* [2010a] discuss in detail the results of 19 May 2006.

[104] We used the particle size distributions and complex refractive indices from the inversion of the Sun photometer data, and we determined single-scattering albedo at 350, 450, and 550 nm. For this purpose we first computed single-scattering albedo at 441, 501, 675, 869, and 1021 nm. We then extrapolated on the basis of a simple linear regression to 350 nm and 450 nm (we use the results at 441 nm and 501 nm). Regarding the results at 550 nm we use the single-scattering albedo at 501 and 675 nm for the linear regression. We assume that the error that is introduced by this simple extrapolation procedure does not introduce additional significant uncertainties at 450 and 550 nm. Additional significant uncertainties may be introduced at 350 nm. Because we do not have the complex refractive index from AERONET at this wavelength we have no means of quality checking. Light-absorption may strongly increase with decreasing wavelength, and for this reason we may overestimate single-scattering albedo from AERONET at 350 nm.

[105] We obtained the single-scattering albedo from measurements with SOAP [*Müller et al.*, 2009]. SOAP provides us with the imaginary part of the complex refractive index. This parameter is given as wavelength dependent quantity. The details of the retrieval procedure are found in the work of *Müller et al.* [2010a].

[106] We find rather good agreement of the data from Sun photometer and SOAP at 550 nm. As in the case of all previous parameters, we again see a difference at the

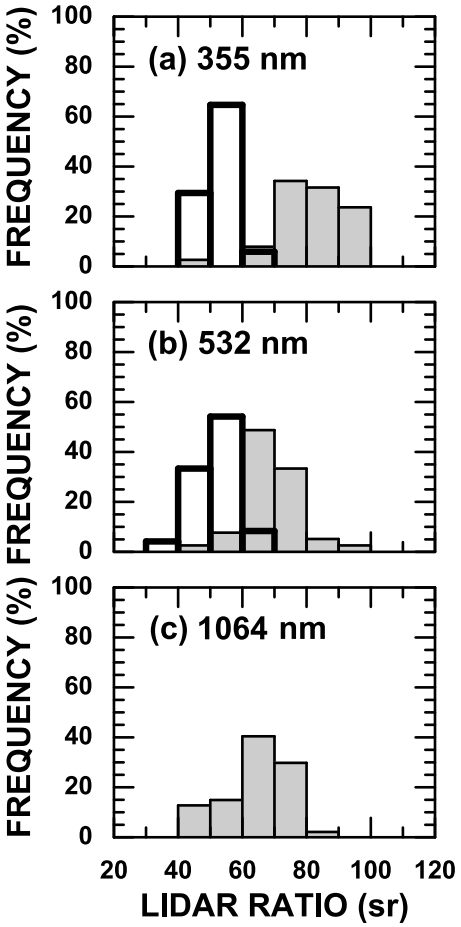

Figure 11. Frequency distributions of lidar ratios at (a) 355 nm, (b) 532 nm, and (c) 1064 nm. Results are shown for AERONET Sun photometer data (grey columns) and lidar measurements (open columns). The results represent the mean of the lidar ratios of the individual samples; 38 samples at 355 nm, 39 samples at 532 nm and 47 samples at 1064 nm.

ultraviolet wavelength at 350 nm. SOAP delivers lower values for the single-scattering albedo than Sun photometer.

[107] Figure 11 summarizes the lidar ratios measured with lidar. Lidar ratios at 355 nm are similar to the lidar ratios at 532 nm. Most of the values range between 50 and 60 sr. Values in the range from 40–50 sr are second most. We do not have measurements of lidar ratios at 1064 nm.

[108] The lidar ratios were computed from the Sun photometer data products at 355, 532, and 1064 nm. We used the particle size distributions and complex refractive indices of the Sun photometer retrievals. For the computations we assumed spheroids and the axis ratio distribution used by AERONET [*Dubovik et al.*, 2006]. The lidar ratios at 355 nm are significantly larger than the measured lidar ratios. Most values range from 70–100 sr, compared to 40–60 sr obtained with lidar. At 532 nm wavelength this difference becomes less pronounced. The lidar ratio distribution inferred from the Sun photometer data at 1064 nm wavelength is rather similar to the one at 532 nm.

[109] There may be several causes for the deviation between lidar and Sun photometer results. A high imaginary part pushes lidar ratios toward higher values. We may hypothesize that the imaginary part inferred from the AERONET data is too large at ultraviolet wavelengths. This assumption however is in contradiction to the fact that the mineralogical analysis of particles suggests an even higher imaginary part at ultraviolet wavelengths; see Figure 3.

[110] We extrapolated the lidar ratios to 355 nm. We applied a linear fit and we used the lidar ratios at 441 and 501 nm. As in the case of the single-scattering albedo, our extrapolation procedure that uses the lidar ratios at 441 and 501 nm may introduce error, because the light-absorption may significantly increase at the shorter wavelengths below 441 nm. However, in this case we see that the AERONET results of lidar ratio are already significantly larger at 355 nm than what we measured with lidar. So in this sense, we obtain an opposite behavior of a possibly larger light-absorption capacity of mineral dust at ultraviolet wavelengths. The Sun photometer values may be high in the case of single-scattering albedo, but they are in fact already too high for the lidar ratio.

[111] Small particles can be another reason for larger lidar ratios. We hypothesize that larger particles, i.e., a larger share of particles in the coarse mode fraction of the dust size distribution could lower the lidar ratio. However, this assumption would be contradictory to the extinction-related Ångström exponents from Sun photometer and lidar, which do not show a neutral spectral dependence of particle extinction. We point out once more that the Sun photometer observations suggest a factor two smaller particle effective radii compared to the in situ observations.

[112] The assumption of size-equivalence in the Sun photometer inversion algorithm may be another reason that can lead to the discrepancies of the lidar ratio. It may be wrong to assume that particles of same size, but different shape can lead to similar optical properties. This assumption may be particularly wrong for parameters that strongly depend on particle shape. The lidar ratio, which describes the extinction-to-backscatter ratio is such a parameter. Particle backscattering depends strongly on particle shape. Thus the use of spheroids, the way it is employed in the Sun photometer inversion algorithm, may cause discrepancies between the computed lidar ratios and the measured lidar ratios. In that regard, also the particle-shape distribution, respectively the aspect ratio distribution may be a reason for the observed discrepancies.

[113] Another reason for the discrepancies of the lidar ratio is that desert dust aerosol is a mixture of absorbing and non-absorbing components [*Kandler et al.*, 2009], but only a single component is considered in the model used by the Sun photometer inversion algorithm. As *Gasteiger et al.* [2011] demonstrate, the non-absorbing components have strong influence on the lidar ratio at short wavelengths.

[114] Figure 12 shows that the particle depolarization ratios from AERONET scatter from low values around 10% (at 355, 532 and 1064 nm) to values as large as 25% at 355 and 532 nm and 35% at 1064 nm. The mean value from lidar at 532 nm is larger than the mean value at 532 nm from Sun photometer. The mean value from lidar at 1064 nm is similar to the mean value at 1064 nm from Sun photometer.

[115] The scatter of values may in part result from measurement uncertainties of the input parameters that are used for the computation of the linear depolarization ratios. In part the lower depolarization ratios may be caused by some contribution from particles in the fine mode fraction of the particle size distribution.

[116] The modeled depolarization ratio tends to lower values than what was measured by lidar at 532 nm. On the basis of all the information on particle size distributions measured aboard the Falcon and at ground during the one month period of SAMUM we have no reason to believe that the fine mode fraction of the particle size distribution is the main cause for the lower depolarization ratios that we inferred from the Sun photometer results.

[117] However, our comparison lacks from a statistical robustness. The AERONET model has not been designed for describing light scattering at 180°. We do not have a sufficient data base regarding the lidar measurements at 355 nm. At 1064 nm we find similar values for the linear particle depolarization ratio. The data base is rather sparse at this wavelength, too.

[118] As already noted by *Müller et al.* [2010b], there seems to be a maximum of the depolarization ratio at 532 nm and lower values at the other two measurement wavelengths. The quality of the lidar measurements of the depolarization ratio was not optimal during SAMUM 2006. We will expand our study to particle depolarization measurements carried out during SAMUM 2008 [*Ansmann et al.*, 2011; *Groβ et al.*, 2011].

4.3. Light-Scattering Computations

[119] Figure 13 shows the aspect ratios of dust particles collected during several Falcon overflights over Ouarzazate. The aspect ratio distribution did not change significantly during 7 overpasses on 4 measurement days. The aspect ratio distribution peaks around 1.5. We show for comparison the aspect ratio distribution used by *Dubovik et al.* [2006]. The frequency of aspect ratios increases with increasing aspect ratio, and it stops at the value 3. In contrast, the aspect ratios measured during the overpasses of the aircraft are as large as 4. However, aspect ratios above 2.5 occur with rather low frequency. *Kandler et al.* [2009] determined the aspect ratios on the basis of particles lying flat on the substrates. The values therefore may not be fully representative of the real

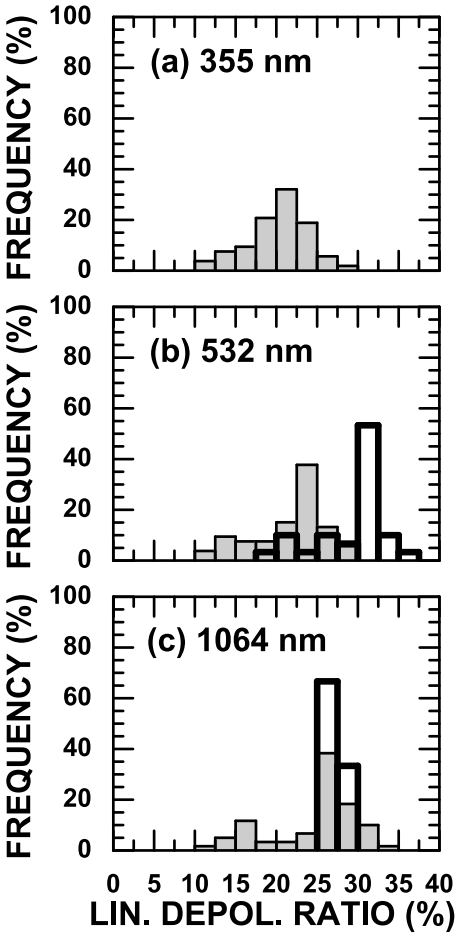

Figure 12. Histogram distributions of the linear dust depolarization ratios at (a) 355 nm, (b) 532 nm, and (c) 1064 nm. Results are shown for AERONET Sun photometer data (grey columns) and lidar measurements (open columns). The results represent the mean of the number of measurement samples listed in Table 3.

distribution. In the context we also refer to *Reid et al.* [2003] who discuss aspect-ratio measurements.

[120] We carried out light-scattering computations. We derived lidar ratios and linear particle depolarization ratios at 355, 532, and 1064 nm. We used the particle size distributions and complex refractive indices inferred from the Falcon measurements and derived from the inversion of the Sun photometer data. We also used the complex refractive indices derived at Tinfou. We used all possible combinations of the particle size distributions (from Sun photometer and from Falcon) and complex refractive indices (from Sun photometer, Falcon, and Tinfou) for the computations. Regarding the imaginary part we have two sets of results for Tinfou. One set of values follows from single-particle analysis. Another set of results follows from SOAP [*Müller et al.*, 2009]. With regard to SOAP we again have two choices. One set of imaginary parts includes the contribution from soot. Another set describes the influence of dust, only.

[121] Figure 14 shows a summary of the computations for one measurement day. A detailed description will be given in a future contribution. We used for the modeling of the optical properties of the single particles the method by *Mishchenko and Travis* [1998] which has been supplemented by the geometric optics approach [*Macke and Mishchenko*, 1996]. The procedure of calculating the optical properties of mixtures is described by *Gasteiger et al.* [2011]. The aspect ratio distribution of *Dubovik et al.* [2006] was applied in the calculations. The particle radii from the in situ measurements were applied as cross-section-equivalent radii, whereas the size distributions from AERONET are given and applied as volume-equivalent sizes. In the first step we computed the parameters for the wavelengths at which we have the complex refractive indices available, which is not necessarily at 355 and/or 532 and/or 1064 nm. For example, from AERONET data we have values at 441, 501, 675, 869, and 1021 nm. In that case we extrapolated with a linear regression to the three lidar wavelengths using the data of the nearest available wavelengths, for example 441 and 501 nm in the case of extrapolation to 355 nm.

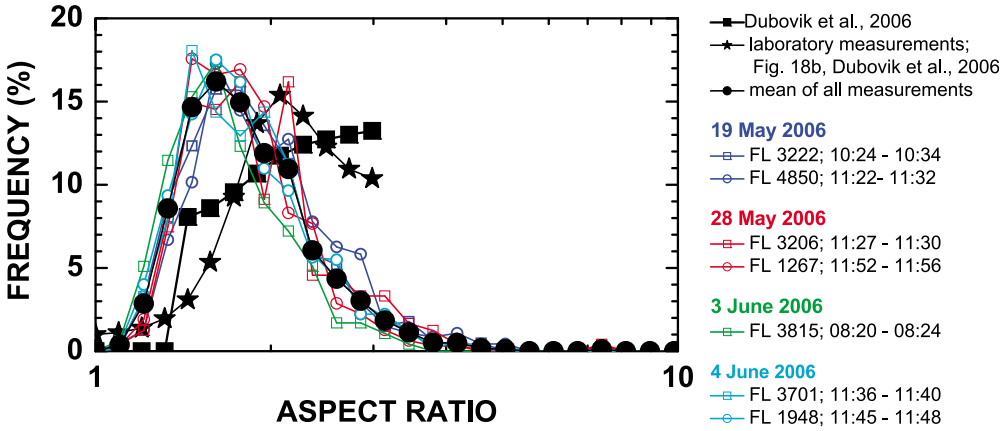

Figure 13. Frequency density distribution of aspect ratios determined from single particle analysis. The meaning of the symbols is given in the legend. FL means flight level. The numbers denote altitude in m. All measurement times are given in UTC. Also shown is the mean axis ratio distribution of all individual measurements carried out during SAMUM 2006 (bullets). For comparison we show the aspect ratio distribution that is used in the AERONET retrieval scheme (black squares). We also show the aspect-ratio distribution measured under laboratory conditions (stars); see *Dubovik et al.* [2006] for details.

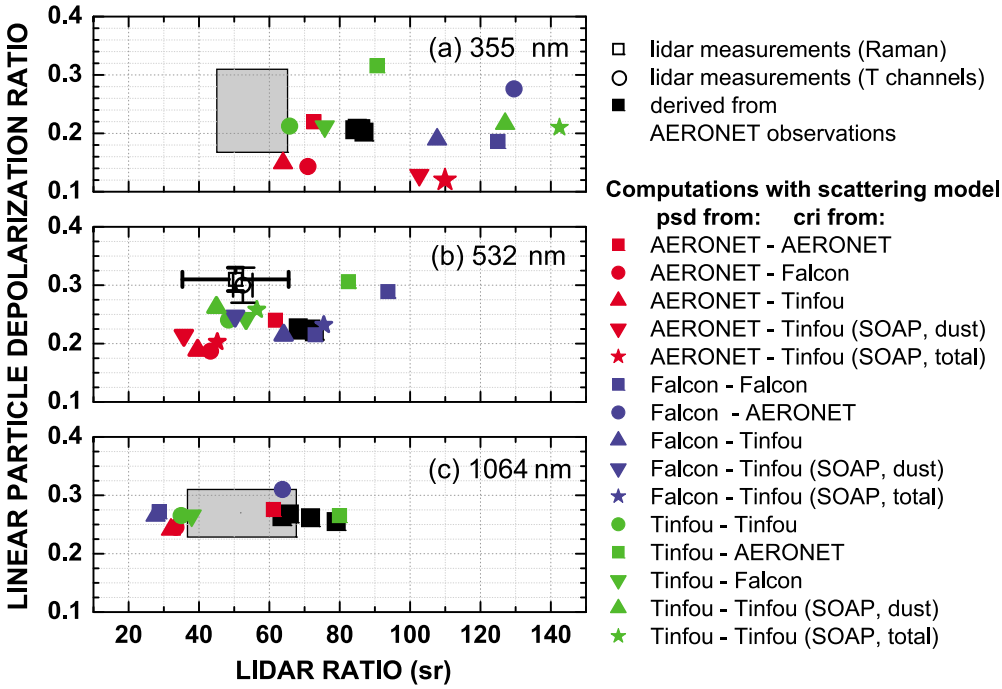

Figure 14. Comparison of lidar measurements of linear particle depolarization ratios and lidar ratios to results from simulations with a light-scattering model [*Wiegner et al.*, 2009; *Gasteiger et al.*, 2011]. Shown are the results at (a) 355 nm, (b) 532 nm, and (c) 1064 nm wavelength. We measured these parameters with lidar on 19 May 2006. The quality of the linear dust depolarization ratios measured with lidar at 355 and 1064 nm is low. We indicate this by the grey shaded boxes. At 532 nm we have high-quality data that allow us to show mean value and standard deviation. For the simulations we use combinations of particle size distributions (psd) and complex refractive indices (cri) measured with the different SAMUM platforms. The results represent the number of samples given in Table 3. The combinations are shown in the legend. The meaning of the abbreviations is as follows: *psd from* means that the measurement of the particle size distribution was done with the respective platform (AERONET Sun photometer, aboard the Falcon aircraft or at ground at Tinfou), and *cri from* means that the complex refractive index was obtained from the respective measurement platforms mentioned for *psd from*, respectively. *SOAP, dust* means means that we used the complex refractive index corrected for the influence of soot. *SOAP, total* means that we also considered the contribution of soot to the complex refractive index. *T channels* means that particle extinction was inferred by the rotational Raman channels of BERTHA under daylight conditions [*Müller et al.*, 2003; *Tesche et al.*, 2009].

[122] The spread of the results gives an impression on the uncertainties of modeled lidar-relevant optical dust properties. These uncertainties result from the uncertainties of the microphysical parameters we derived from the different measurement platforms. This result in fact points out to a problem of the field measurements, which may be at the root of the observed discrepancies. Each platform by itself gives a consistent set of microphysical and optical properties. But it may be impossible to mix results on parameters obtained from different measurement platforms. This means, for example, it may not be feasible that we use particle size distribution measurements from AERONET in combination with refractive indices retrieved from mineralogical analysis for the computation of, e.g., the lidar ratio.

[123] The linear particle depolarization ratios and lidar ratios measured with lidar at 355 nm and 532 nm do not overlap with the results of the computations in the sense that the lidar derived values are centered inside the range of all computed lidar ratios and linear particle depolarization ratios. We show the results at 1064 nm for completeness. Our lidar data set is too small to allow for any trustworthy conclusion on the quality of the computations at each wavelength.

[124] The depolarization ratios measured with lidar tend to be at the upper end of values depicted in Figure 14. The lidar ratios measured with lidar at 355 nm are lower than what is found from the simulation studies at 355 nm. Regarding the lidar ratio at 532 nm the situation looks more favorable. The simulation results are within the variability measured with lidar.

[125] The aspect ratio distribution has some influence on the linear particle depolarization ratio. Computations with spheroids of various size parameters show that the linear depolarization ratio changes [see *Gasteiger*, 2011, Figure 3.2]. We do not find a correlation in the sense that higher aspect ratios result in higher depolarization ratios, or vice versa.

5. Summary and Conclusions

[126] In this third part of our series of quality assurance tests of the SAMUM 2006 results we compare data of the

complete measurement period. We compare in detail data that were collected on four days. On these days nearly every measurement platform provided data. We also present a statistical overview on some of the parameters that were observed by AERONET, Raman lidar, high-spectral-resolution lidar, and in situ instruments during the one-month measurement period.

[127] We find differences that likely are not the result of different measurement times. For example, the intensive properties of the dust plumes showed comparably little variation throughout the campaign [e.g., *Kandler et al.*, 2009; *Müller et al.*, 2009; *Tesche et al.*, 2009; *Weinzierl et al.*, 2009]. We find systematic differences for particle size distribution, and thus particle effective radius, complex refractive index (also the wavelength dependence), and important optical dust properties like absorption and scattering coefficients, lidar ratios and depolarization ratios.

[128] We investigated lidar ratios and depolarization ratios with a data base that contains scattering properties of dust particles. This data bank contains results for the parameters computed from the size distributions and complex refractive index which were derived with the various instrument platforms. We find a large scatter for lidar ratios and linear particle depolarization ratios, when we combine the different size distributions and complex refractive indices. Lidar measures lidar ratio and depolarization ratio directly. The results that use AERONET parameters do not coincide with the results measured by lidar.

[129] SAMUM offers us deep insight into several open questions of remote sensing of mineral dust and the retrieval of optical and microphysical dust parameters. This insight was in great part achieved through coordinated activities of airborne and ground-based remote sensing instrumentation and airborne in situ measurements. SAMUM shows discrepancies among dust parameters which likely have to be attributed to the fact that none of the employed methods can derive a complete set of dust parameters by itself. Secondary data products are computed from primary data products, e.g., absorption coefficients follow from measurements of particle size distributions and complex refractive indices. The assumptions that have to be made in the retrievals of the secondary data products generate uncertainties which are unacceptably large in view of the demands of the modeling community regarding climate forcing studies.

[130] We summarize our studies into the following lessons:

[131] 1. A set of particle parameters (microphysical and optical properties) is consistent in itself as long as we derive this set of parameters from the same platform. This means: microphysical parameters (particle size distribution and complex refractive index) from Sun photometer reproduce the dust optical properties (optical depth, single-scattering albedo, scattering and absorption coefficients). Falcon microphysical parameters reproduce the optical properties measured with nephelometer and PSAP. Note that desert dust is a mixture of different minerals, each having a different complex refractive index. Our comparisons suggest that the "effective" complex refractive index of such mixtures may depend on the measurement principle.

[132] 2. Regardless of this consistency of parameters within one measurement platform we observe significant off-set of the same microphysical and optical parameters among different measurement platforms. For instance, complex refractive index from Sun photometer is systematically lower than the one derived from mineralogical analysis of single particles.

[133] 3. It remains an open question if the wavelength-dependence of the complex refractive index can be derived with sufficient accuracy so that it can be used for an accurate computation of dust optical properties and radiative forcing studies. We find in part significant differences of the wavelength-dependencies of the imaginary parts from AERONET Sun photometer, SOAP, and mineralogical analysis of particles. We believe that the correct description of particle shape in data analysis may not be the only reason of the observed differences. Each measurement method may deliver a different wavelength dependence, for example because of different measurement respectively retrieval sensitivities in the different wavelength ranges these methods use. Furthermore, mineral dust consists of different chemical components and the final value for the imaginary part describes this composition in terms of an effective value. This effective value again may depend on the methodology, as each method may exhibit stronger detection sensitivity to specific chemical components that are contained in the particles, respectively.

[134] 4. It remains an open question if any retrieval of the imaginary part can be verified with another measurement method that rests upon a different physical measurement principle. The statement on the complex refractive index can be summarized as follows: we still lack in useful methods that allow us to infer the complex refractive index on the basis of first principles.

[135] 5. Aircraft measurements of particle scattering and absorption with nephelometer and PSAP, respectively, are not designed for inferring these parameters across a sufficiently broad wavelength range. A significant extension of the measurement wavelength range would be necessary for retrieving particle extinction coefficients at (near) ultraviolet wavelengths (strong light-absorption by dust) and near infrared wavelengths. Only if this extension is done we could perform a useful comparison with AERONET Sun photometer and Raman lidar.

[136] 6. There is a mismatch of absorption and scattering coefficients between AERONET Sun photometer and Falcon aircraft. Regarding the Sun photometer data we believe that an insufficient description of the wavelength dependence of these parameters, which in fact is related to an insufficient description of the wavelength-dependence of the imaginary part, is responsible for absorption coefficients that are too low at ultraviolet wavelengths. It would be useful, if AERONET could provide complex refractive indices at wavelengths shorter than 441 nm on an operational basis. This extension could benefit instruments that operate at UV wavelengths like lidar. We are aware that this wavelength extension may not be straightforward to achieve. Regarding the airborne measurements it is clear that the measurement wavelength of around 450 nm (nephelometer, PSAP) is insufficient to derive absorption coefficients at shorter wavelengths, which would be urgently needed.

[137] 7. We lack in powerful methods that allow us to obtain a reasonable link between retrieval results (optical and/or microphysical parameters) from remote sensing data and results from so-called in situ observations across sufficiently wide ranges of measurement wavelengths. We need

to employ measurement strategies in field missions that allow us to test if the different methods provide similar (same) results across a wide range of wavelengths from the near ultraviolet region to the near infrared region. We need to learn more about measurement and retrieval uncertainties and how the uncertainties change with, for example measurement wavelength. In this context we point out to publications from, e.g. *Leahy et al.* [2007] and *Johnson et al.* [2009] who show reasonable agreement of single-scattering albedo of smoke and mixtures of smoke and dust observed with Sun photometer and in situ instrumentation. *Toledano et al.* [2011] also find reasonable agreement of single-scattering albedo for mixtures of smoke with dust observed over the Cape Verde Islands during the Saharan Mineral Dust Experiment in 2008 [*Ansmann et al.*, 2011]. Single-scattering albedo of the SAMUM 2006 data which describes pure mineral dust does not match as well.

[138] 8. We find systematically higher particle volume concentrations from in situ measurements aboard Falcon compared to the volume size distributions retrieved with AERONET. Our uncertainty computations of the in situ size distributions show that the choice of the complex refractive index, which is needed in the retrieval of the Falcon particle size distributions, has impact at particle radii above 2 μm. But this effect still cannot account for the observed gross differences. It remains an open issue to what extend particle shape has influence on the airborne in situ measurements, and this question needs to be tackled in future field experiments. We consider this point particularly important in view of results by *Osborne et al.* [2008] who also show that airborne in situ size distributions of dust particles are shifted toward larger particle radii compared to AERONET derived size distributions.

[139] 9. Particle aspect ratio distributions from microscopic observations are different from the distributions used by the AERONET algorithm. It remains an open issue if the aspect ratio distribution is a critical factor in the retrieval of the AERONET data products.

[140] 10. SAMUM cannot answer the question if spheroids with smooth surface are the best possible choice in retrieving dust parameters that depend strongly on particle shape, like lidar ratios and depolarization ratios. However, it is obvious that any kind of light-scattering computations assuming spherical particles should be avoided in data analysis of dust measurements. This particularly applies to in situ measurements where it is still a common approach to use spherical particle shape in data analysis.

[141] 11. It seems unlikely that dust lidar ratios from Sun photometer retrievals can be used as trustworthy input in the analysis of data collected with so-called backscatter lidars. Even though we find a reasonable match of lidar ratios at 532 nm to the ones measured with Raman lidar, there simply remains too much uncertainty on the general applicability of Sun photometer for retrievals of this parameter. There is a strong mismatch of the lidar ratio measured at 355 nm with Raman lidar to the lidar ratio inferred from Sun photometer data.

[142] 12. Lidar measures particle depolarization ratios and lidar ratios without assumption on particle shape. For this reason, Raman lidar and high-spectral resolution lidar must be the method of choice for any verification of these parameters by any other remote sensing or in situ measurement method.

6. Future Progress

[143] In view of the studies we carried out until now and summarizing the results of the SAMUM-2006 field campaign (special issue on SAMUM in Tellus, 61 B, 2009) we need field campaigns that could help in further resolving the problems connected with the modeling of optical properties of mineral dust. We need novel instrumentation and we need to further improve the measurement strategy we developed during SAMUM. Otherwise open questions, as for instance *which light-scattering model is appropriate for describing optical properties of mineral dust?* will not be answered.

[144] If we want to make significant progress in dust research with remote sensing methods we must combine airborne observations of particles with ground-based and airborne remote sensing instrumentation. Lidar has to be part of such studies. This method does not require knowledge of particle shape for measurements of some optical properties of mineral dust. The overlap range [*Wandinger and Ansmann*, 2002] of such lidars must be as close to the ground as possible. Thus, we also need Sun photometer at the lidar site as it can efficiently compensate for the overlap effect, and it delivers high-quality optical depth data, aside from additional products like microphysical properties. This Sun photometer should be operated with the measurement channel at 1638 nm.

[145] A novel field experiment on pure mineral dust (or mixtures of dust with other pollution types) should make use of a new airborne multiwavelength lidar which could solve many problems that are connected to ground-based lidar systems. The ideal candidate for such a lidar would be an airborne multiwavelength high-spectral-resolution lidar that delivers backscatter and extinction coefficients at several wavelengths plus depolarization information at one or more wavelengths at day- and nighttime [*Burton et al.*, 2012; *Hair et al.*, 2008; *Rogers et al.*, 2009].

[146] We also need airborne in situ instrumentation which must cover a broad range of particle sizes, at least up to 15 μm particle radius. We must measure the fine mode fraction, too, in order to rule out that particle size distribution measurements are "contaminated" by anthropogenic pollution.

[147] Particles need to be collected in various flight levels for subsequent mineralogical analysis and determination of aspect ratios, the way it was done during SAMUM 2006. Novel instruments for measurement of the state of polarization of light scattered by the airborne dust particles would fill gaps in our knowledge of optical properties. An airborne version of SOAP [*Müller et al.*, 2009] would be highly beneficial for spectrally resolved measurements of particle light-absorption, particularly at near UV wavelengths. The data must be taken in coordinated actions among the different platforms.

[148] We may go much further with our measurement strategy and request for novel instrument technology. In another step this airborne multiwavelength high-spectral-resolution lidar should fly over a site that is equipped with two ground-based lidar systems which should either be Raman lidar (nighttime measurements of extinction only) or high-spectral-resolution lidar (daytime and nighttime observations

of extinction coefficients). In the most ideal case the two ground-based lidars should also be multiwavelength systems for backscatter, extinction and depolarization ratio measurements, and at least one system should be able to measure in a wavelength range larger than the currently used upper limit of 1064 nm. For example laser wavelengths and detection channels around 1600–2000 nm could be tackled in the future.

[149] The first ground-based system should emit the laser beam(s) vertically. The second ground-based system should not only emit its own laser beam(s), but this second system should be operated several kilometers away from this first ground-based lidar. The most suitable distance depends on dust layer height over the first ground-based system. The signal-receiver system of this second ground-based system must have a scanning unit such that it can scan along the laser beam that is emitted vertically by the first ground-based system. The signal-detection unit of this second system must be able to detect the laser radiation that is scattered to the sides of the vertically outgoing laser beam of the first system. Clearly, such an instrument set-up requires sophisticated alignment and synchronization of the two systems regarding the laser-pulse emission unit and the signal detection unit.

[150] In the end we obtain a sophisticated bi-static lidar set-up that could permit us to measure sideward-scattered laser radiation. It is clear that we can measure with the second, scanning system, at each height level of the vertically emitted laser beam laser radiation at one sideward scattering angle only. However, if the dust plume is high enough and homogeneous, we will be able to reconstruct the particle scattering phase function for a specific range of scattering angles on the basis of radiation measured at different scattering angles in different height ranges at one or more wavelengths.

[151] Finally this second, scanning system, should also measure the signal of the laser radiation it emits itself. Particularly along the line of the vertically pointing laser beam of the first system we thus would also obtain particle backscatter and extinction coefficients which could serve as a powerful tool of quality assurance of the overall set of data collected with these two systems.

[152] In summary, this idea goes far beyond any field campaign that has been designed so far. We had plans of carrying out tests of such instrument configurations during SAMUM-2006 as some of the lidar instrumentation was available. The lack of preparation time and the lack of time during the field campaign did not allow us to do this work.

[153] **Acknowledgments.** This study was funded by CATER 2009-3112. The SAMUM campaign was funded by the German Research Foundation (Deutsche Forschungsgemeinschaft) within the Research Group SAMUM under grant FOR 539. We thank Oleg Dubovik and the AERONET team at Goddard Space Flight Center for providing us with high-quality Sun photometer results. We are grateful to the Moroccan Ministry for Foreign Affairs and the Ministry of the Interior for their permission to carry out the SAMUM field campaign in Morocco. We thank the Moroccan Airport Authority and in particular respectable Monsieur Mohammed El Mardi, commander of Ouarzazate airport, for their extraordinary support of the participants of SAMUM.

References

Althausen, D., D. Müller, A. Ansmann, U. Wandinger, H. Hube, E. Clauder, and S. Zörner (2000), Scanning 6-wavelength 11-channel aerosol lidar, *J. Atmos. Ocean. Tech.*, *17*, 1469–1482.

Ansmann, A., A. Petzold, K. Kandler, I. Tegen, M. Wendisch, D. Müller, B. Weinzierl, T. Müller, and J. Heintzenberg (2011), Saharan Mineral Dust Experiments SAMUM-1 and SAMUM-2: What can be learned from these dust closure field campaigns?, *Tellus, Ser. B*, *63*, 403–429, doi:10.1111/j.1600-0889.2011.00555.x.

Bergstrom, R. W., P. Pilewskie, P. Russell, J. Redemann, T. C. Bond, P. K. Quinn, and B. Sierau (2007), Spectral absorption properties of atmospheric aerosols, *Atmos. Chem. Phys.*, *7*, 5937–5943.

Böckmann, C., I. Miranova, D. Müller, L. Scheidenbach, and R. Nessler (2005), Microphysical aerosol parameters from multiwavelength lidar, *J. Opt. Soc. Am.-A*, *22*, 518–528.

Burton, S. P., R. A. Ferrare, C. A. Hostetler, J. W. Hair, R. R. Rogers, M. D. Obland, C. F. Butler, A. L. Cook, D. B. Harper, and K. D. Froyd (2012), Aerosol classification system using airborne High Spectral Resolution Lidar measurements: Methodology and examples, *Atmos. Meas. Tech.*, *5*, 73–98, doi:10.5194/amt-5-73-2012.

Cattrall, C., J. Reagan, K. Thome, and O. Dubovik (2005), Variability of aerosol and spectral lidar and backscatter and extinction ratios of key aerosol types derived from selected Aerosol Robotic Network locations, *J. Geophys. Res.*, *110*, D10S11, doi:10.1029/2004JD005124.

Coen, M. C., E. Weingartner, D. Schaub, C. Hueglin, C. Corrigan, S. Henning, M. Schikowski, and U. Baltensperger (2004), Saharan dust events at the Jungfraujoch: Detection by wavelength dependence of the single scattering albedo and first climatology analysis, *Atmos. Chem. Phys.*, *4*, 2465–2480.

Dubovik, O., and M. D. King (2000), A flexible inversion algorithm for retrieval of aerosol optical properties from Sun and sky radiance measurements, *J. Geophys. Res.*, *105*, 20,673–20,696.

Dubovik, O., et al. (2006), The application of spheroid models to account for aerosol particle nonsphericity in remote sensing of desert dust, *J. Geophys. Res.*, *111*, D11208, doi:10.1029/2005JD006619.

Eck, T. F., B. N. Holben, J. S. Reid, O. Dubovik, A. Smirnov, N. T. O'Neill, I. Slutsker, and S. Kinne (1999), Wavelength dependence of the optical depth of biomass burning, urban, and desert dust aerosols, *J. Geophys. Res.*, *104*, 31,333–31,350.

Esselborn, M., M. Wirth, A. Fix, B. Weinzierl, K. Rasp, M. Tesche, A. Petzold, and G. Ehret (2009), Spatial distribution and optical properties of Saharan dust observed by airborne high spectral resolution lidar during SAMUM 2006, *Tellus, Ser. B*, *61*, 131–143, doi:10.1111/j.1600-0889.2008.00394.x.

Fialho, P., A. D. A. Hansen, and R. E. Honrath (2005), Absorption coefficients by aerosols in remote areas: A new approach to decouple dust and black carbon absorption coefficients using seven-wavelength Aethalometer data, *J. Atmos. Sci.*, *36*, 267–282.

Freudenthaler, V., et al. (2009), Depolarization-ratio profiling at several wavelengths in pure Saharan dust during SAMUM 2006, *Tellus, Ser. B*, *61*, 165–179.

Gasteiger, J. K. (2011), Retrieval of microphysical properties of desert dust and volcanic ash aerosols from ground-based remote sensing, diss., 137 pp., Universität München, Munich, Germany.

Gasteiger, J., M. Wiegner, S. Gross, V. Freudenthaler, C. Toledano, M. Tesche, and K. Kandler (2011), Modelling lidar-relevant optical properties of complex mineral dust aerosols, *Tellus, Ser. B*, *63*, 725–741, doi:10.1111/j.1600-0889.2011.00559.x.

Groβ, S., et al. (2011), Characterization of the planetary boundary layer during SAMUM-2 by means of lidar measurements, *Tellus, Ser. B*, *63*, 695–705, doi:10.1111/j.1600-0889.2011.00557.x.

Hair, J. W., C. A. Hostetler, A. L. Cook, D. B. Harper, R. A. Ferrare, T. L. Mack, W. Welch, L. R. Izquierdo, and F. E. Hovis (2008), Airborne high-spectral-resolution lidar for profiling aerosol optical profiles, *Appl. Opt.*, *47*, 6734–6752, doi:10.1364/AO.47.006734.

Heese, B., D. Althausen, T. Dinter, M. Esselborn, T. Müller, M. Tesche, and M. Wiegner (2009), Vertically resolved dust optical properties during SAMUM: Tinfou compared to Ouarzazate, *Tellus, Ser. B*, *61*, 195–205.

Holben, B. N., et al. (1998), AERONET: A federated instrument network and data archive for aerosol characterization, *Remote Sens. Environ.*, *66*, 1–16.

Holben, B. N., et al. (2001), An emerging ground-based aerosol climatology: Aerosol optical depth from AERONET, *J. Geophys. Res.*, *106*, 12,067–12,097.

Huang, J., N. C. Hsu, S. Tsay, M.-J. Jeong, B. N. Holben, T. A. Berkoff, and E. J. Welton (2011), Susceptibility of aerosol optical thickness retrievals to thin cirrus contamination during the BASE-ASIA campaign, *J. Geophys. Res.*, *116*, D08214, doi:10.1029/2010JD014910.

Johnson, B. T., S. Christopher, J. M. Haywood, S. R. Osborne, S. McFarlane, C. Hsu, C. Salustro, and R. Kahn (2009), Measurements of aerosol properties from aircraft, satellite and ground-based remote sensing: a case-study from the Dust and Biomass-burning Experiment (DABEX), *Q. J. R. Meteorol. Soc*, *135*, 922–934.

Kandler, K., et al. (2009), Size distribution, mass concentrations, chemical and mineralogical composition, and derived optical parameters of the boundary layer at Tinfou, Morocco, during SAMUM 2006, *Tellus, Ser. B*, *61*, 32–50.

Kandler, K., et al. (2011), Ground-based off-line measurements at Praia, Cape Verde, during the Saharan Mineral Dust Experiment: Microphysical properties and mineralogy, *Tellus, Ser. B*, *63*, 725–741, doi:10.1111/j.1600-0889.2011.00559.x.

Knippertz, P., et al. (2009), Dust mobilization and transport in the northern Sahara during SAMUM 2006, *Tellus, Ser. B*, *61*, 12–31.

Leahy, L. V., T. L. Anderson, T. F. Eck, and R. W. Bergstrom (2007), A synthesis of single scattering albedo of biomass burning aerosol over southern Africa during SAFARI 2000, *Geophys. Res. Lett.*, *34*, L12814, doi:10.1029/2007GL029697.

Macke, A., and M. I. Mishchenko (1996), Applicability of regular shapes in light scattering calculations for atmospheric ice particles, *Appl. Opt.*, *35*, 4291–4296, doi:10.1364/AO.35.004291.

Mishchenko, M. I., and L. D. Travis (1998), Capabilities and limitations of a current Fortran implementation of the T-matrix method for randomly oriented rotationally symmetric scatterers, *J. Quant. Spectrosc. Radiat. Transfer*, *60*, 309–324.

Müller, D., U. Wandinger, and A. Ansmann (1999a), Microphysical particle parameters from extinction and backscatter lidar data by inversion with regularization: Theory, *Appl. Opt.*, *38*, 2346–2357.

Müller, D., U. Wandinger, and A. Ansmann (1999b), Microphysical particle parameters from extinction and backscatter lidar data by inversion with regularization: Simulation, *Appl. Opt.*, *38*, 2358–2368.

Müller, D., I. Mattis, U. Wandinger, D. Althausen, A. Ansmann, O. Dubovik, S. Eckhardt, and A. Stohl (2003), Saharan dust over a central European EARLINET-AERONET site: Combined observations with Raman lidar and Sun photometer, *J. Geophys. Res.*, *108*(D12), 4345, doi:10.1029/2002JD002918.

Müller, D., I. Mattis, A. Ansmann, U. Wandinger, C. Ritter, and D. Kaiser (2007), Multiwavelength Raman lidar observations of particle growth during long-range transport of forest-fire smoke in the free troposphere, *Geophys. Res. Lett.*, *34*, L05803, doi:10.1029/2006GL027936.

Müller, D., et al. (2010a), Mineral dust observed with AERONET Sun photometer, Raman lidar, and in situ instruments during SAMUM 2006: Shape-independent particle properties, *J. Geophys. Res.*, *115*, D07202, doi:10.1029/2009JD012520.

Müller, D., et al. (2010b), Mineral dust observed with AERONET Sun photometer, Raman lidar, and in-situ measurements during SAMUM 2006: Shape-dependent particle properties, *J. Geophys. Res.*, *115*, D11207, doi:10.1029/2009JD012523.

Müller, T., A. Schladitz, A. Maßling, N. Kaaden, A. Wiedensohler, and K. Kandler (2009), Spectral absorption coefficients and imaginary parts of refractive indices of Saharan dust during SAMUM-1, *Tellus, Ser. B*, *61*, 79–95.

Osborne, S. R., B. T. Johnson, J. M. Haywood, A. J. Baran, M. A. J. Harrison, and C. L. McConnel (2008), Physical and optical properties of mineral dust aerosol during the Dust and Biomass-burning Experiment, *J. Geophys. Res.*, *113*, D00C03, doi:10.1029/2007JD009551.

Petzold, A., et al. (2009), Saharan dust refractive index and optical properties from aircraft-based observations during SAMUM 2006, *Tellus, Ser. B*, *61*, 118–130.

Reid, J. S., et al. (2003), Comparison of size and morphological measurements of coarse mode dust particles from Africa, *J. Geophys. Res.*, *108*(D19), 8593, doi:10.1029/2002JD002485.

Reid, J. S., E. A. Reid, A. Walker, S. Piketh, S. Cliff, A. A. Mandoos, S.-C. Tsay, and T. F. Eck (2008), Dynamics of southwest Asian dust particle size characteristics with implications for global dust research, *J. Geophys. Res.*, *113*, D14212, doi:10.1029/2007JD009752.

Rogers, R. R., et al. (2009), NASA LaRC airborne high spectral resolution lidar aerosol measurements during MILAGRO: Observations and validation, *Atmos. Chem. Phys.*, *9*, 4811–4826.

Russell, P. B., et al. (2010), Absorption Angstrom Exponent in AERONET and related data as an indicator of aerosol composition, *Atmos. Chem. Phys.*, *10*, 1155–1169.

Tesche, M., et al. (2009), Vertical profiling of Saharan dust with Raman lidars and airborne HSRL in southern Morocco during SAMUM, *Tellus, Ser. B*, *61*, 144–164.

Toledano, C., M. Wiegner, M. Garhammer, M. Seefeldner, V. Freudenthaler, J. Gasteiger, D. Müller, and P. Köpke (2009), Spectral aerosol optical depth characterization of desert dust during SAMUM 2006, *Tellus, Ser. B*, *61*, 216–228.

Toledano, C., et al. (2011), Optical properties of aerosol mixtures derived from Sun-sky radiometry during SAMUM-2, *Tellus, Ser. B*, *63*, 635–648, doi:10.1111/j.1600-0889.2011.00573.x.

Veselovskii, I., A. Kolgotin, V. Griaznov, D. Müller, U. Wandinger, and D. N. Whiteman (2002), Inversion with regularization for the retrieval of tropospheric aerosol parameters from multiwavelength lidar sounding, *Appl. Opt.*, *41*, 3685–3699.

Veselovskii, I., O. Dubovik, A. Kolgotin, T. Lapyonok, P. D. Girolamo, D. Summa, D. N. Whiteman, M. I. Mishchenko, and D. Tanré (2010), Application of randomly oriented spheroids for retrieval of dust particle parameters from multiwavelength lidar measurements, *J. Geophys. Res.*, *115*, D21203, doi:10.1029/2010JD014139.

Wandinger, U., and A. Ansmann (2002), Experimental determination of the lidar overlap profile with Raman lidar, *Appl. Opt.*, *41*, 511–514.

Weinzierl, B., A. Petzold, M. Esselborn, M. Wirth, K. Rasp, K. Kandler, L. Schütz, P. Köpke, and M. Fiebig (2009), Airborne measurements of dust layer properties, particle size distribution and mixing state of Saharan dust during SAMUM 2006, *Tellus, Ser. B*, *61*, 96–117.

Wiegner, M., et al. (2009), Numerical simulations of optical properties of Saharan dust aerosols with emphasis on linear depolarization ratio, *Tellus, Ser. B*, *61*, 180–194.

D. Althausen, A. Ansmann, D. Müller (corresponding author), and T. Müller, Leibniz Institute for Tropospheric Research, Permoserstr. 15, D-04318 Leipzig, Germany. (dietrich@tropos.de; albert@tropos.de; detlef@tropos.de; muellert@tropos.de)

J. Gasteiger, Meteorological Institute, Ludwig Maximilian University, Theresienstr. 37, D-80333 Munich, Germany. (josef.gasteiger@lmu.de)

K. Kandler, Institut für Angewandte Umweltwissenschaften, Technische Universität Darmstadt, D-64287 Darmstadt, Germany. (kzk@gmx.de)

K.-H. Lee, Atmospheric Remote Sensing Laboratory, School of Environmental Science and Engineering, GIST, 123 Cheomdan-gwagiro (Oryong-dong), Buk-gu, Gwangju 500-712, South Korea. (lkh1515@gist.ac.kr)

S. Otto, Leipzig Institute for Meteorology, University of Leipzig, Stephanstr. 3, D-04103 Leipzig, Germany. (sebastian.otto@uni-leipzig.de)

M. Tesche, ITM, Stockholm University, Svante Arrhenius väg 8, SE-10691 Stockholm, Sweden. (matthias.tesche@itm.su.se)

C. Toledano, Grupo de Óptica Atmosférica, Universidad de Valladolid, Prado de la Magdalena s/n, E-47071 Valladolid, Spain. (toledano@goa.uva.es)

B. Weinzierl, Institut für Physik der Atmosphäre, DLR, D-82234 Wessling, Germany. (bernadett.weinzierl@dlr.de)